HOST UNIVERSITY: The University of Edinburgh

FACULTY: College of Science and Engineering

DEPARTMENT: Civil & Environmental Engineering

Academic Year 2020-2021

The performance of shear studs in solid and composite slabs at ambient and elevated temperatures

Mina Mikhail

Supervisor: Prof. Grunde Jomaas

Master thesis submitted in the Erasmus+ Study Programme

International Master of Science in Fire Safety Engineering

Disclaimer

This thesis is submitted in partial fulfilment of the requirements for the degree of *The International Master of Science in Fire Safety Engineering (IMFSE)*. This thesis has never been submitted for any degree or examination to any other University/programme. The author(s) declare(s) that this thesis is original work except where stated. This declaration constitutes an assertion that full and accurate references and citations have been included for all material, directly included and indirectly contributing to the thesis. The author(s) gives (give) permission to make this master thesis available for consultation and to copy parts of this master thesis for personal use. In the case of any other use, the limitations of the copyright have to be respected, in particular with regard to the obligation to state expressly the source when quoting results from this master thesis. The thesis supervisor must be informed when data or results are used.

Read and approved,
Mina Mikhail

May 11, 2021

Acknowledgements

I would like to express my sincere gratitude to my supervisor and personal tutor Prof. Grunde Jomaas for his help, support, patience and his continuous motivation that pushed me further throughout the whole period of this dissertation.

Special thanks are dedicated to ARUP for suggesting the starting point for this thesis and to Yavor Panev as an industrial supervisor from their side.

Last but not the least, I am greatly thankful for my parents and my sister who have always been supporting and praying for my success. It would not have been possible for me to complete my studies without their support and love during this unprecedent time of the pandemic.

Abstract

Numerical modelling was conducted with ABAQUS to investigate the performance of the headed shear studs in solid and composite slabs at normal temperatures. In addition, a thermo-mechanical analysis was carried out to study the behaviour of the stud at elevated temperatures in the solid slab. For the composite slab, a three-dimensional FE model was developed to study the behaviour of the headed studs with the corrugated metal sheeting with ribs oriented parallel to the beam to resemble main beams supporting a typical slab of a building. The typical push-out tests were simulated using the ABAQUS/Explicit solver which is convenient for this type of analysis, as complex interactions between different elements and damage problems are encountered. The material of concrete was modelled using the concrete damaged plasticity available in the ABAQUS library and a perfect plastic stress-strain curve was used for the steel material of the headed stud. The capacity of the studs as well as the load-slip curves were established from the results of the model. The numerical capacity of the studs was compared with the strength predictions of Eurocode 4. The numerical model was validated using the numerical results obtained by Lam and El lobody (2005), Chen et al. (2016) and Mirza and Uy (2009). It was found that the failure mode in the slab is dominated by the steel stud failure rather than the concrete cone failure. Also, the predicted capacities from Eurocode 4 appeared to be conservative if the recommended value for the partial factor was used. At elevated temperatures, the stud reached 25 % of its strength at ambient temperature. Furthermore, the results were proven to be very sensitive to the parameters used in the model as well as the loading rate applied in the explicit solver.

Nomenclature

R_{sc} : capacity of the headed shear stud (N)

f_u : ultimate tensile strength of the stud (MPa)

d_{sc} : shank diameter of the stud (mm)

γ_v : partial factor for design shear resistance of a headed stud

f_{ck} : characteristic cylinder compressive strength of the concrete at 28 days (MPa)

f_{cm}: mean value of concrete cylinder compressive strength (MPa)

E_{cm} : secant modulus of elasticity of concrete (MPa)

α : reduction factor used when the mean height of the weld collar is less than $\frac{d_{sc}}{5}$

h_{sc} : overall nominal height of the stud (mm)

n_r: number of stud connectors in one rib

$k_{u,\theta}$: reduction factor for the yield strength of structural steel giving the strain hardening

stress level at elevated temperature $f_{au,\theta}$

$f_{au,\theta}$: ultimate tensile strength of structural steel or steel for stud connectors in the fire situation, allowing for strain-hardening (MPa)

$k_{c,\theta}$: reduction factor for the compressive strength of concrete giving the strength at elevated temperature $f_{c,\theta}$

$f_{c,\theta}$: characteristic value for the compressive cylinder strength of concrete in the fire situation at temperature θ °C (MPa)

$\gamma_{M,fi,v}$: partial factor for the shear resistance of stud connectors in the fire situation

f_c : compressive stress in concrete (MPa)

σ_t : tensile stress in concrete (MPa)

f_t : maximum tensile stress of concrete (MPa)

ε : strain in concrete

ε_{co} : strain at ultimate stress of concrete

$\varepsilon^{\sim in}$: compressive inelastic strain

$\varepsilon^{\sim pl}$: compressive plastic strain

d_c : compressive damage variable of concrete in the concrete damaged plasticity model

d_t : tensile damage variable of concrete in the concrete damaged plasticity model

w : crack opening displacement (mm)

w_c : ultimate crack opening displacement (mm)

f_{cmo} : base value of mean compressive cylinder strength (MPa)

G_f : fracture energy needed to form a unit area of crack

G_{fo} : base value of the fracture energy

λ_c : thermal conductivity of concrete (W/mK)

λ_s : thermal conductivity of steel (W/mK)

θ_c : concrete temperature

α_c : coefficient of thermal expansion of concrete

α_s : coefficient of thermal expansion of steel

$\varepsilon_{c,\theta}$: concrete strain at temperature θ_c

$\varepsilon_{cu,\theta}$: concrete strain at stress equal to $f_{c,\theta}$

Relevant terminology worth defining from Eurocode 4 (EC4)

The design of composite members and structures where members are joined together to withstand loads is referred to in Eurocode 4 "En1994-1-2". Typically, the members and structures are made of reinforced or pre-stressed concrete and structural steel.

Composite member

"A structural member with components of concrete and of structural or cold-formed steel, interconnected by a shear connection so as to limit the longitudinal slip between concrete and steel and the separation of one component from the other."

Shear connection

"An interconnection between the concrete and steel components of a composite member that has sufficient strength and stiffness to enable the two components to be designed as parts of a single structural member."

Composite behaviour

"It is the behaviour which occurs after the shear connection has become effective due to the hardening of concrete

Table of Contents

List of Figures

List of tables

1. Introduction

In recent decades, steel and concrete composite slabs have been widely used in constructing high-rise buildings. The shear stud has been the most common type used of shear connectors between steel and concrete in composite girders over the years due to its economic advantage. From a fire safety point of view, the complexity of the behaviour of the composite structures is a topic of interest. Many concerns and issues are still investigated in the research field when it comes to predicting the behaviour of these complex structures. This topic became essential especially after the successive collapses of the world trade center (WTC) buildings on 11th of September. Referring to the report of the National Institute of Standards and Technology (NIST), several conclusions are drawn on the contribution of structural components in failure initiation are unexpected and have raised concerns (NIST, 2008). These conclusions include the role of both shear studs and local-global buckling of the floor beams in failure initiation. It was pointed out that the failure of the shear studs in the composite floors exerted large deformations at the connection between a girder and a column. Forces from thermal expansion failed the connection at the column, then pushed the girder off the seat. This resulted in the loss of lateral support for the column which made the column to buckle followed by a progression failure of floor systems and then pulled down the rest of the building (McAllister *et al.*, 2013).
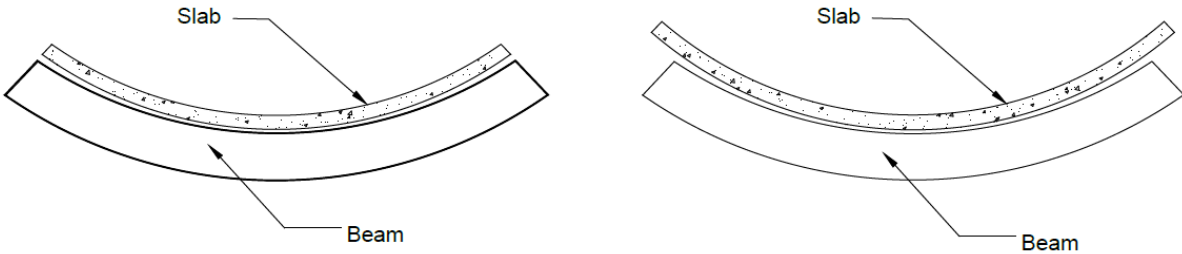
Fig. 1: Differential thermal expansion between a beam and a slab, composite action (left), no composite action (right) (Flint et al., 2013)

The breakage of shear studs is considered an issue due to many aspects. A technical aspect was pointed out by Flint et al. (2013) that comprise various points. The breakage of shear studs is a major concern in the composite slabs as it can lead to different restraint patterns and deflection in the slab unlike full composite interaction. In addition, the shear stud is considered the link between the beam and the slab and if this link is broken, an overall reduction in the floor system strength takes place. Many consequences tend to occur as a result of this breakage. Loss of anchoring the slab to the primary structure makes the slab lateral movement possible over the supporting beams causing the slab to slide in toward the bays with the largest spans, deflections and/or loads. Also, the slab thermal curvature can only be driven by the differential temperatures in the slab and beam individually as a result of this breakage. The lateral-torsional failure of the beam is more likely to happen as the slab also helps to keep the beams in line (Flint et al., 2013).

Membrane action of composite slabs

The breakage of shear studs has raised a technical and an economical aspect when the demand for transforming the structural fire design to follow a performance-based approach rather than a prescriptive approach has been increasing in the previous years. The reason for this is to fairly evaluate the performance of individual elements and to assess the response of a building in real fire scenarios. The performance-based approach allows a better understanding of the actual behaviour of the building in a fire. Besides, it gives the flexibility to apply fire protection only to specific elements that must be protected and not all of the elements. In return, an economical advantage is achieved by saving time, materials and reduction in weight of the structure.

One of these applications is relying on the membrane action under accidental fire loads of the composite slabs as it provides additional resistance during a fire. In this design method, the secondary beams could be left unprotected without experiencing a structural collapse of the slab but only experiencing a high deflection. When a fire occurs, the membrane action is established and the static load is transferred from the unprotected secondary beams to the protected main beams. (Bailey, 2004)

To guarantee that the slab will perform in this behaviour during the fire, an assumption is made by Bailey (2004) in this design approach which is the transfer of the tensile force from the beam to the composite slab through shear connectors. Also, these forces should be resisted by the compressive membrane generated around the slab's perimeter. Accordingly, for the application of this design method, the performance of the shear connectors must be thoroughly investigated to ensure the transfer of the forces from the beam to the composite slab under fire conditions. Bailey (2004) described this slab panel behaviour as a bicycle wheel in which the spokes represent the tensile membrane action and the wheel rim represents the compressive membrane action. For the development of the membrane action, the beams within the floor are designed so that plastic hinges should not be formed in the beams and the flexural resistance of the slab is maintained by the slab panel behaviour.
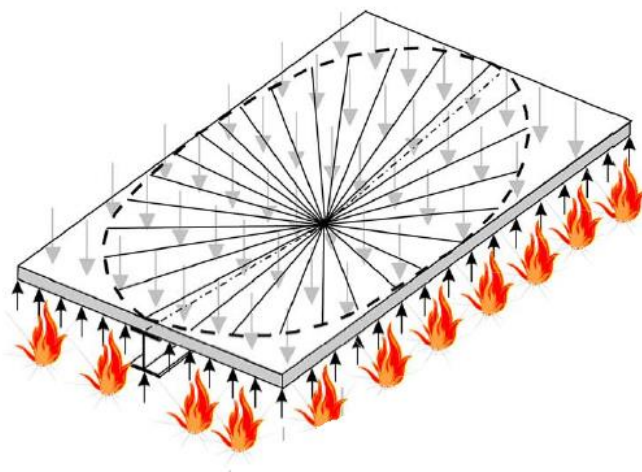
Fig. 2: Behaviour mode with a fan yield pattern for the membrane action of a composite floor slab (Bailey, 2004)

1.1 Concepts of composite action

Composite beams usually consist of a hot rolled steel section (I-section for example) with shear connectors welded along the top flange of the beam to achieve the composite interaction between the beam and the concrete slab. Various types of shear connectors can be used for the composite interaction but normally headed shear studs are used. Composite slabs are commonly used with composite beams. The composite slab consists of a steel decking that is supported by the composite beams. The steel decking is reinforced in-situ and

the concrete was cast on the steel decking which acts as formwork for concrete. When the concrete is hardened, the two elements act as one due to the presence of the shear connectors and the decking which contributes to the shear bond with the concrete as well (Rackham, 2014).

Shear connectors are the key element to ensure a composite mechanism between the steel and concrete at the interface in between. They are important for the transmission of the shear forces between the steel and concrete so that they act as one element. Their effectiveness is crucial for the composite members to withstand the applied loads. The main concept is to take the advantages of concrete in compression and the high tensile strength of steel in tension. The steel beam is placed in the tension side to avoid buckling of steel in compression. Similarly, the concrete slab is placed in the compression side to avoid the weakness of concrete in tension. By bonding the steel beam to the concrete slab, the moment capacity of the whole section will be at least doubled with a significant increase in the stiffness of the beam. As a result of increasing the capacity and the stiffness, the beam spans can be increased and there will be a reduction in the deflection of the slab and the depth of the beam.

In the case of assuming that there is a full shear connection between concrete and steel, there must be a horizontal displacement (slip) between concrete and steel to transfer the shear force although there is a full shear connection. This is known as the shear interaction which is different from the shear connection. In the case of partial interaction, there should be two separate neutral axes one for concrete and the other for steel section. And as the degree of shear interaction increases until it reaches full interaction, there should be only one neutral axis for the whole composite section Accordingly, it is considered that the shear connector transmits all the horizontal forces between steel and concrete. (Oehlers *et al.*, 1997).

1.2 Types of shear connectors (historical background)

There are various types and forms of shear connectors that could be welded to the top flange. They were originally used in bridges construction back in the 1920s when this type of composite structures started. They are divided into ductile (studs and spiral), semi-ductile (channels and angles) and non-ductile (I-section, T-section, C-section). Spiral shear

connectors were later replaced by channels to provide the composite action between steel and concrete in steel bridges. The three types of shear connections have different load-slippage curves as indicated in Fig. 4.
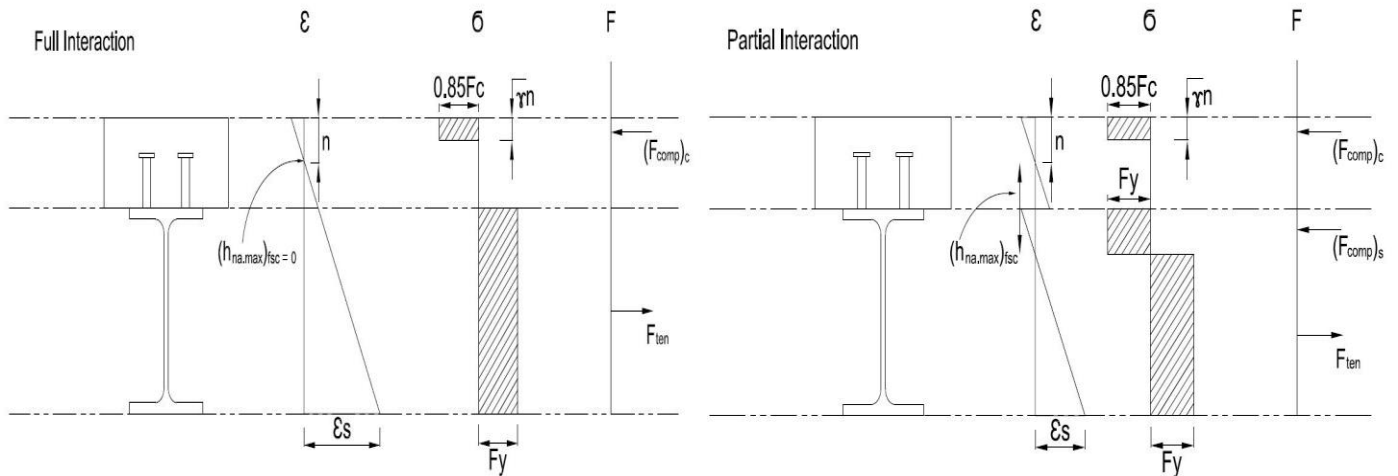
Fig. 3: Composite section with partial interaction (left) and full interaction (right) (Oehlers *et al.*, 1997)

Typically, the full composite action between the concrete slab and steel beam results in economic and structural benefits as discussed earlier. Theoretically, this could be only achieved if the relative slippage at the interface between the steel beam flange and the slab is nil. Nevertheless, practically, a slippage is often witnessed due to the ductile behaviour of the shear stud while transferring the shear force.

Also, other forms of shear connectors are developed to provide resistance in both vertical and horizontal direction such as (Perfobond ribs, Oscillating-perfobond strip and Waveform-strip). These forms contribute differently to shear transfer and uplift prevention. They have different performance according to the type of concrete used whether it is normal weight concrete, lightweight concrete, concrete with fibres or high strength concrete.
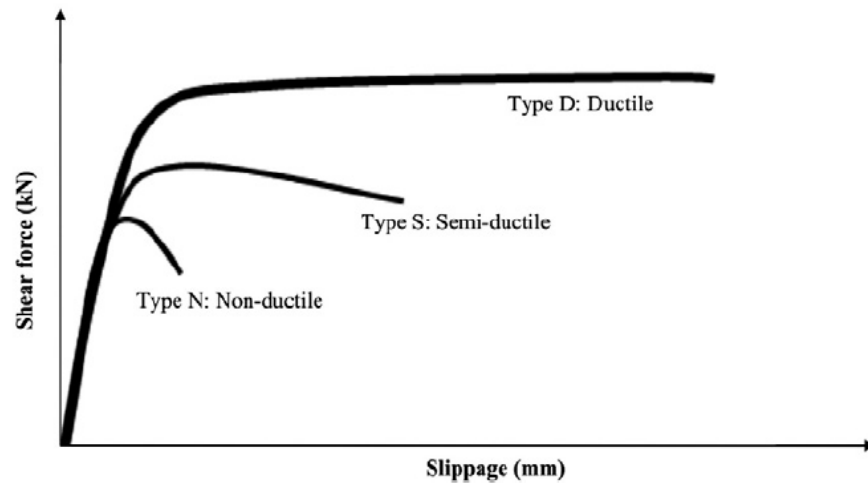
Fig. 4: load- slippage curves for different types of shear connectors (Shen and Chung, 2017)
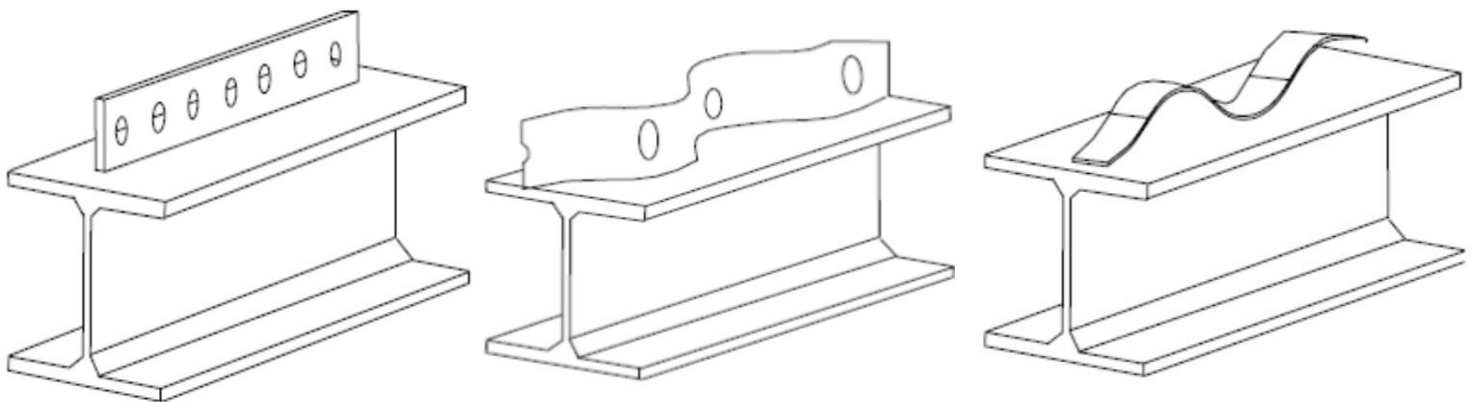
Fig. 5: Illustrations of Perfobond (left), Oscillating-perfobond (middle) and Waveform-strip shear connectors (right) (Ali Shariati, 2012)

1.2.1 Headed shear studs

A shear stud consists of a head, a shank and the weld-collar to attach the shank to the steel flange. The shank and weld-collar are primarily designed to resist the longitudinal shear forces, while the head is designed to engage with the concrete and to resist the tensile force perpendicular to the interface between the steel and the concrete. This tensile force (uplift force) is due to the bending of the beam and its tendency to separate from the slab. The mechanical performance of shear studs is assessed through the load and the relative slip at

the interface between steel and concrete at the point of connection of the stud. The shank diameter of headed studs ranges from 10 mm to 22 mm (19 mm is the most commonly used). The length of headed studs before welding varies from 55 mm to 250 mm (3 mm to 11 mm will be decreased after welding). (Zaki et al., 2003), (J W Rackham, 2014)
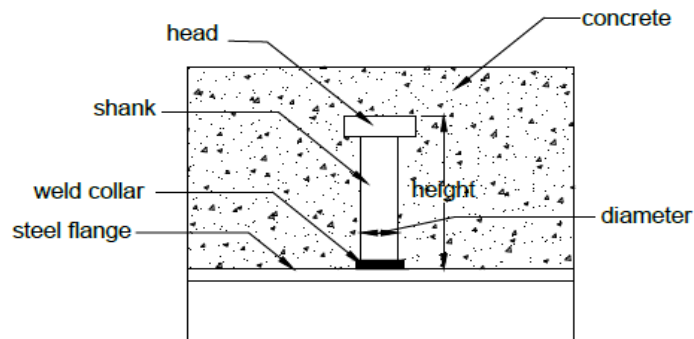
Fig. 6: headed shear stud by (Oehlers and Bradford, 1995)

Shear studs welded to the top flange of beams are considered the commonly used application in composite beams. The shear studs are always welded to the steel flange in both cases whether using a solid concrete slab or a composite slab with a ribbed steel metal deck. In the case of using a composite slab, the headed studs are welded through the metal deck. Ribs of the metal deck could be fixed either parallel or transverse to the steel beam. Detailed cross-section drawings of such configurations are illustrated as shown in Fig. 7
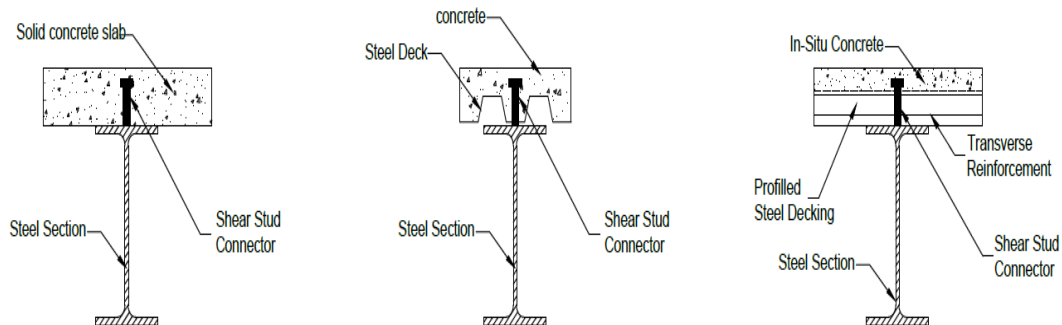
Fig. 7: headed stud fixed in the solid slab (left), composite slab with ribs parallel to the I-beam (middle) and composite slab with ribs transverse to the I-beam (right)

According to (Oehlers and Bradford, 1995) the shear stud is subjected to shear and flexural forces at the bottom of the stud. These forces arise as a reaction to resist the slippage of the beam from the concrete when the beam is loaded. The concrete area surrounding the bottom of the stud should bear high compressive stresses to restrain the movement of the stud. The force causing these stresses should be in equilibrium with shear force in the steel section. Therefore, a couple is formed at the base which made the stud to resist both bending and shear forces.

1.3   Push-out test

This test is prescribed in Eurocode 4 as the standard test on shear connectors that provides information on the properties of shear connection required for design. Usually, push-out testing is utilized to develop the load-slip curves of the stud such that a pure shear force is applied to the stud, but ideally load-slip behaviour should be obtained from full-scale beam tests. It is argued that this standard test does not fully represent the bending behaviour of composite beams. This is due to the fact that a significant redistribution of load to the less stressed studs is witnessed in the composite beam full-test which makes the studs have an enhanced strength and ductility compared to the push-out tests. Nevertheless, analysing the behaviour of studs in beams is complicated and it has been observed by researchers that developing force-slip curves from push-out tests are adequate(Vasif Atilla Oven, 1996).

1.4   Load-slip curve of stud at ambient temperature

The force on the Y-axis is the normalised force (force/ ultimate strength of the stud) and the slippage is the recorded displacement in (mm) that occurs between the steel section and the concrete face. The relationship between the force and the slip by Chapman and Balakrishnan (1964) is divided into 3 regions which are elastic, transition region and plastic. The elastic part is up to 55 % of the ultimate capacity of the studs followed by the transition region and the perfect plastic part over 95 % of the ultimate capacity of stud.

1-cover 15 mm

2-bedded in mortar or gypsum

3-recess optional

4-reinforcement: ribbed bars Ø 10 mm
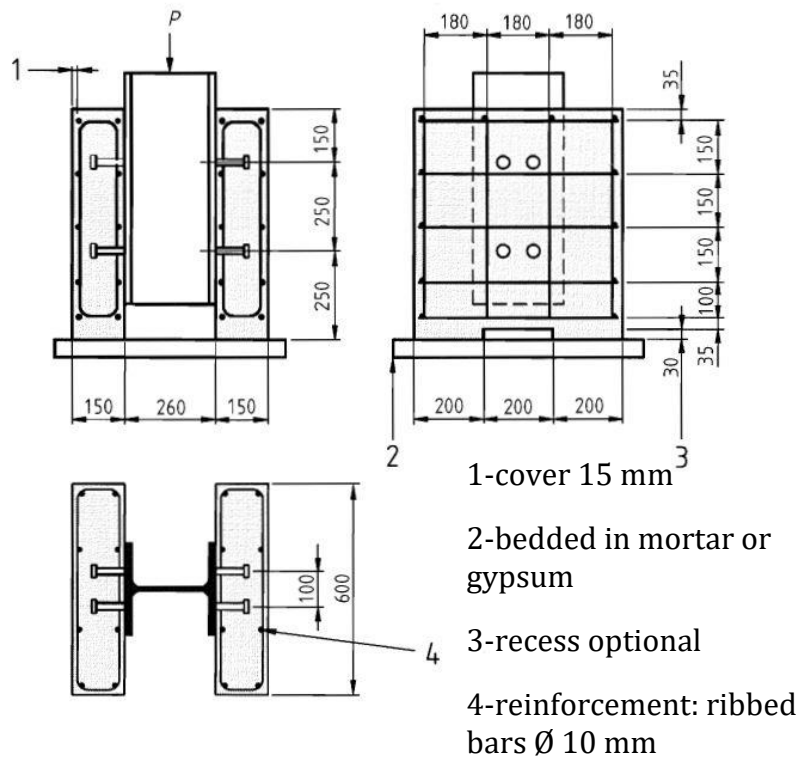
Fig. 8: Standard push-out test according to Eurocode 4
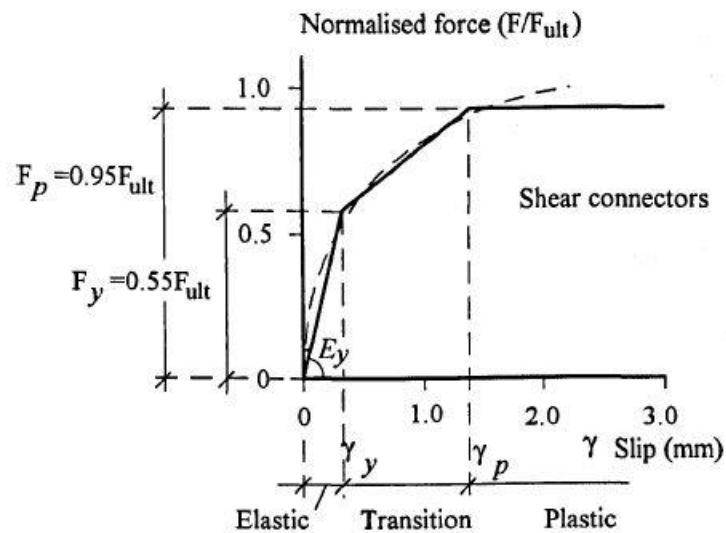
Fig. 9: Force-slip curve at ambient temperature (Chapman and Balakrishnan, 1964)

The load-slip curve of a shear connector is usually nonlinear, and the shear connector stiffness has no solid definition. This is because of the scatter in this value when compared to other variables. Previous studies discussed the difficulty to find any regression formula for shear connector stiffness. In order to quantify the results, the ultimate load that was reached in the load-slip curve should not be used directly in design calculations since it imposes extremely high relative slippage on a composite structure that might not be able to withstand. An approach was proposed to take the design resistance as 80% of the ultimate resistance, and the stiffness is conservatively estimated as the secant stiffness at the design strength with an equivalent slip of 0.8 mm (Wang, 1998).

1.5 Strength of headed Shear stud prediction equations

The capacity of the shear stud depends on the properties of the stud itself and the material properties of the concrete slab in which it is embedded. This is due to the fact that the capacity of the stud is restricted either by the shear strength of the stud or by the strength of the concrete in contact with and around the stud to transfer the shear force. The strength of shear stud is function of the concrete properties which are compressive strength, tensile strength, the modulus of elasticity, and concrete density. It is also function of the properties of studs including tensile strength and the diameter of studs and numbers as well. The capacity is also influenced by the type of the slab decking, decking orientation, type of aggregate used and the position of the stud in the trough of the deck.

1.5.1 Design resistance of shear stud in solid slabs at ambient conditions according to Eurocode 4 "En1994-1-2"

The shear capacity of the welded headed shear stud could be calculated from Eq. (1) or Eq. (2) whichever is the smaller:

$$R_{sc} = \frac{0.8\, f_u\, \pi\; d_{sc}^{\,2}}{4\gamma_v} \qquad\qquad \text{Eq. (1)}$$

OR:

$$R_{sc} = \frac{0.29 \, \alpha \, d_{sc}^{2} \sqrt{f_{ck} \, E_{cm}}}{\gamma_{v}}$$

Eq. (2)

$$\alpha = 0.2 \left(\frac{h_{sc}}{d_{sc}} + 1\right) \text{ for } 3 \leq \frac{h_{sc}}{d_{sc}} \leq 4$$

Eq. (3)

$$\alpha = 1 \text{ for } \frac{h_{sc}}{d_{sc}} > 4$$

Eq. (4)

$$E_{cm}(Gpa) = 22\left(\frac{f_{cm}}{10}\right)^{0.3}$$

Eq. (5)

$$f_{cm} = f_{ck} + 8$$

Eq. (6)

Where:

R_{sc} : capacity of the headed shear stud (N)

f_{u} : ultimate tensile strength of the stud but not greater than 500 N/mm² (MPa)

d_{sc} : shank diameter of the stud (mm)

γ_{v} : Partial factor for design shear resistance of a headed stud (recommended value is 1.25)

f_{ck} : characteristic cylinder compressive strength of the concrete at 28 days, of density not less than 1750 kg/m3 (MPa)

f_{cm}: Mean value of concrete cylinder compressive strength (MPa)

E_{cm} : Secant modulus of elasticity of concrete (MPa)

α : reduction factor used when the mean height of the weld collar is less than $\frac{d_{sc}}{5}$

h_{sc} : overall nominal height of the stud (mm)

1.5.2 Design resistance of shear studs with profiled steel sheeting according to Eurocode 4

1.5.2.1 Sheeting with ribs parallel to the supporting beams

The studs are fixed within the trough of the sheeting which has the shape of a haunch. The width of the haunch b_0 is defined as the width of the trough as shown in

Fig. 10. The depth of the haunch is indicated as h_p. The height of the stud is h_{sc} from the base of the trough but not greater than h_p +75 mm as advised by Eurocode 4.
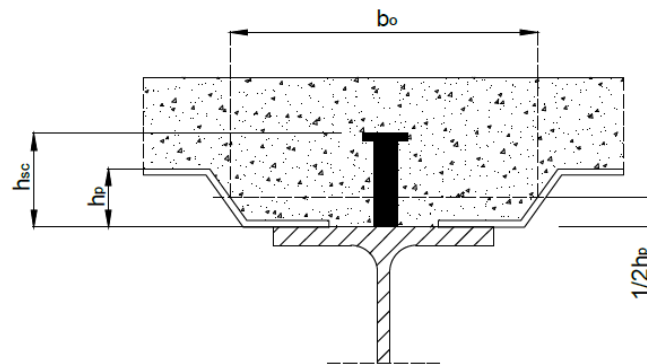
Fig. 10: Trough geometry with parallel ribs from EC4

The capacity of the headed studs in the profiled steel sheeting is the same as the one for the solid slab but only multiplied by a reduction factor K_t given by the following expression:

$$k_t = 0.6 \frac{b_0}{h_p} \left(\frac{h_{sc}}{h_p} - 1 \right) \leq 1$$

Eq. (7)

1.5.2.2 Sheeting with ribs transverse to the supporting beams
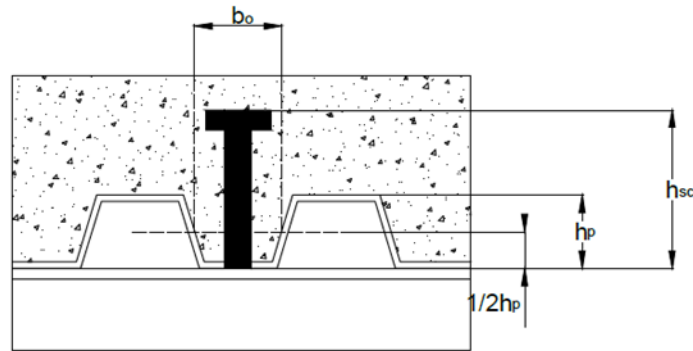
Fig. 11: Trough geometry with transverse ribs from EC4 "En1994-1-2"

The capacity of the headed studs in the profiled steel sheeting with transverse ribs is the same as the one for the solid slab but also multiplied by a reduction factor K_t given by the following expression:

$$k_t = \frac{0.7}{\sqrt{n_r}} \frac{b_0}{h_p} \left(\frac{h_{sc}}{h_p} - 1 \right)$$

Eq. (8)

Where:

n_r: number of stud connectors in one rib (should not exceed 2 in the reduction factor)

Some conditions have to be followed for applying these factors regarding the height and diameter of the studs mentioned in Eurocode 4 "section 6.6.4.2" and "table 6.2" for the upper limits of the reduction factor.

The reduction in the capacity of the studs in the case of using the transverse ribs sheeting is due to the limited available area of the concrete in front of the stud where the force transferred to the slab is relying on to avoid concrete crushing. Conversely, in the case of solid slabs, this area in front of the stud is free (not restrained by the deck profile ribs). That

is why the equation should be adjusted to encounter the geometry of the decking profile. (Rackham, 2014)

1.5.3 Design resistance of shear stud in solid and composite slabs at elevated temperatures according to Eurocode 4

According to Eurocode 4 "En1994-2-2", the shear capacity of the welded headed shear stud in the fire situation could be determined using the equations described in "En1994-1-2" except that the partial factor γ_v should be replaced by $\gamma_{M,fi,v}$. The shear strength could be calculated from Eq. (9) or Eq. (11) whichever is the smaller:

$$R_{sc,fi} = 0.8 \, k_{u,\theta} \, R_{sc}$$

Eq. (9)

$$R_{sc} = \frac{0.8 \, f_u \, \pi \, d_{sc}^2}{4\gamma_{M,fi,v}}$$

Eq. (10)

OR:

$$R_{sc,fi} = k_{c,\theta} \, R_{sc}$$

Eq. (11)

$$R_{sc,fi} = \frac{0.29 \, \alpha \, d_{sc}^2 \sqrt{f_{ck} \, E_c}}{\gamma_{M,fi,v}}$$

Eq. (12)

Where:

$k_{u,\theta}$: reduction factor for the yield strength of structural steel giving the strain hardening stress level at elevated temperature $f_{au,\theta}$

$f_{au,\theta}$: ultimate tensile strength of structural steel or steel for stud connectors in the fire situation, allowing for strain-hardening (MPa)

$k_{c,\theta}$: reduction factor for the compressive strength of concrete giving the strength at elevated temperature $f_{c,\theta}$

$f_{c,\theta}$: characteristic value for the compressive cylinder strength of concrete in the fire situation at temperature θ °C (MPa)

$\gamma_{M,fi,v}$: partial factor for the shear resistance of stud connectors in the fire situation and taken as unity

1.6 Load-slip curves of stud at elevated temperatures

The load-slip behaviour of the stud up to 100 °C is quite similar to the one at normal temperature. It has the same significant features of the 3 regions as discussed earlier. Beyond that, (Kruppa and Zhao, 1995) developed normalised force/slip curves for the headed studs (19 mm ×100 mm) at elevated temperatures. These curves demonstrate the non-linear performance at high temperatures with a slight decrease in the ultimate shear strength till 300 °C as shown in Fig. 12.
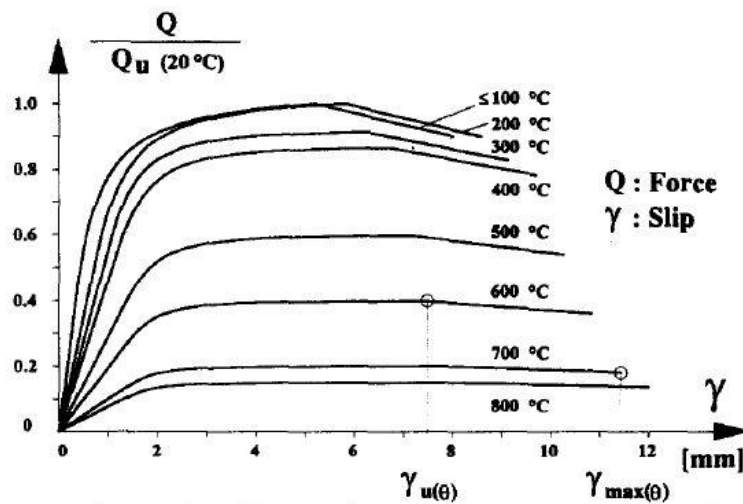
Fig. 12: Normalized force-slip curves at elevated temperatures for 19×100 mm studs by , (Kruppa and Zhao, 1995)

1.7 Previous studies on the behaviour of shear stud in solid and composite slabs at normal and elevated temperatures

In this section, the literature of the previous research investigations reported is going to be elucidated and compared on the performance of shear studs in solid concrete slabs and composite slabs at normal and elevated temperatures. Results from the push-out tests performed at normal and elevated temperatures are explained.

To investigate the complex interaction between different components in composite slabs at elevated temperatures, the different failure modes of solid slabs at normal temperatures is first studied. This is done to better understand the complexities of behaviour at elevated temperatures. Conclusions and failure modes of solid slabs at normal and elevated temperatures by former researchers will be discussed first.

Lam and El-Lobody (2005) performed push-out tests according to the procedures specified in the Eurocode 4 to investigate the behaviour of headed shear studs at normal temperature and to study the different failure modes of headed studs embedded into solid concrete slabs. Besides, they established a 3D finite element model using ABAQUS software to compare the results with the push-out tests. Four test specimens of concrete slabs were used with different compressive strengths and the load-slip curves were developed. The diameter of the headed studs used in the 4 specimens is 19 mm with a 100 mm shank height which turned up to 95 mm after welding. The steel flanges were not greased so the natural bond between the slab and flanges is maintained. The maximum yield strength of the studs used is 470.8 N/mm^2. They concluded that the lower the strength of the solid concrete slab, the more likely the concrete failure. Typically, the load failure is governed by the failure of the concrete area around the stud. However, for higher concrete slab strength, the failure occurred in the studs by shearing-off. For medium strength concrete, concrete failure is accompanied by yielding near the stud collar. These different failure modes were well-predicted by the models in ABAQUS. Summary of the test results are shown in Table 1

Table 1: Comparison of Test Results and Finite Element Solution (Lam and El-Lobody, 2005)

Test reference	Diameter of headed stud (mm)	Concrete strength (MPa)	Push-off test capacity result (KN)	FE model capacity result (KN)
SP1	19	50	130.4	116.6
SP2	19	20	71.6	74.4
SP3	19	30	93	91.8
SP4	19	35	102	97.3

Summary of failure modes of shear studs at normal temperatures for solid slabs observed by Lam and El-Lobody (2005)

- Shear studs shearing off (stud shank failure) with no observation of concrete crushing around the studs (for this typical shank failure, the ultimate capacity of studs is reached before the concrete reaches its compressive strength)
- Concrete cone failure which is a separation of a cone of concrete from the rest of the slab but remained around the stud.
- Concrete cone failure and stud yielding near the stud collar

Choi et al. (2009) conducted modified push-out tests on headed studs with solid slab where the steel section is exposed to fire from 3 sides, unlike the standard set-up. The experiment aims to investigate the performance of headed studs in fire and to identify the strength properties of the stud at room temperature, 30 and 60 minutes inside the heated furnace. The electric furnace was used on one side of the solid slab and the furnace was heated according to the standard ISO 834 curve. The dimensions of the studs used are 19 mm diameter ×100 mm height which is the most commonly used. The compressive strength of the concrete slab is 30 MPa. The steel flanges are greased to prevent the bond between the slab before the concrete cast. The yield strength of the studs used is 349 N/mm² and the ultimate tensile strength of 427 N/mm². They examined the failure

mechanism of the slab at elevated temperatures which was always the shearing off of the stud at the weld collar and shank interface. Choi et al. (2009) has attributed this to the higher temperature development in the area in contact with the heated top flange section.
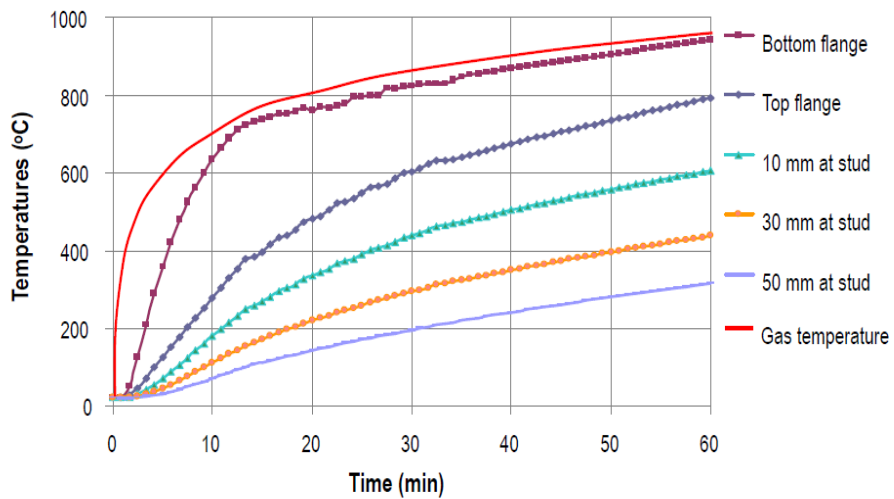
Fig. 13: Time-Temperature curves in steel and stud connector for standard fire (Choi et al., 2009)
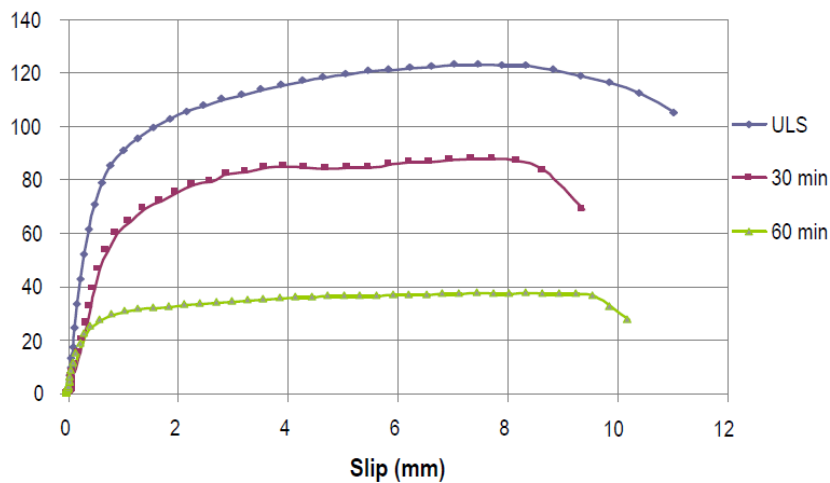
Fig. 14: Load-slip curves for stud connectors at elevated temperatures and ultimate limit state(ULS) (Choi et al., 2009)

Imagawa et al. (2012) performed three different types of push-out tests to understand the static behaviour of headed shear studs before, during and after heating. The test setup comprises a steel member with an H-section and a reinforced concrete slab of width 400 mm and 250 mm depth. The cylinder compressive strength of concrete after 28 days was 32 MPa with a secant modulus of elasticity of 3×10^4 MPa. The dimensions of the studs used were 22 mm diameter and 150 mm height which were higher than the values that are commonly used. The ultimate tensile strength of the shear stud material was 400 MPa. The specimens were tested without heating, heating up to 300°C, heating up to 500°C and finally heating up to 700°C. The heating tests were conducted for up to 90 minutes. The experimental set-up is illustrated in Fig. 15.
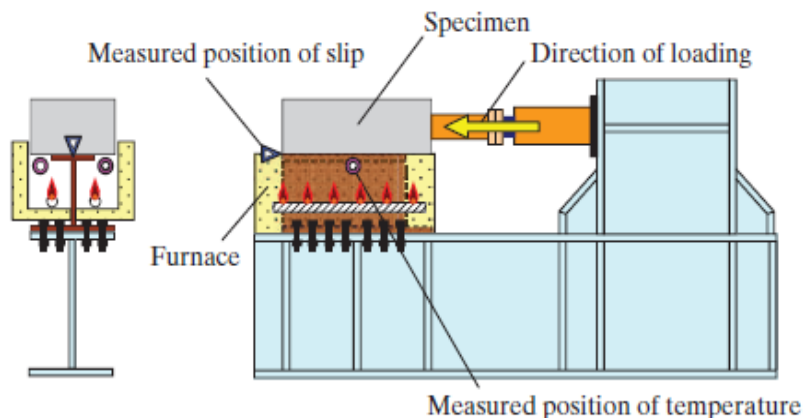
Fig. 15: experimental set-up (Imagawa et al., 2012)

They concluded that during the heating of the shear studs, the shear capacity reduced by 25 % compared to the studs tested at normal temperature. Additionally, the shear resistance values obtained from the experiments well-matched the design values recommended by Eurocode 4. Regarding the failure modes, all the specimens tested under heating conditions experienced a failure mode in the headed stud shanks.

To evaluate the mechanical performance of the shear studs after being exposed to fire and then testing them after being cooled down, another test set-up was conducted such that specimens were separated into two parts. The two parts were firstly heated in the furnace for 90 minutes and then left to be cooled down naturally to normal temperature. Thereafter,

the push-out test was performed on the specimens after being attached according to the procedure shown in Fig. 16
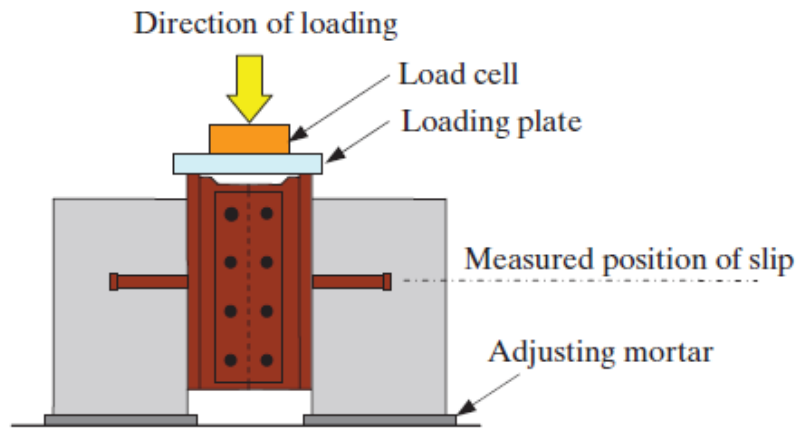
Fig. 16: The push-out testing method after cooling (Imagawa et al., 2012)

Imagawa et al. (2012) observed the following conclusions after heating the specimen to 700°C and cooling:

- The stud's shear resistance dropped down by 25 %
- Values of shear resistance were higher than the design values in Eurocode 4
- The tensile and yield strength of the stud did not decrease much after cooling
- Compressive and modulus of elasticity of concrete decreased when concrete cooled down which affected the results of the push-out test
- Concrete crushing around stud's base which interpreted the reduction in the relative slip
- The state of failure was always observed in the concrete and not in the headed studs.

Chen et al. (2015) performed 24 push-out tests on headed studs with solid slabs, composite slabs with ribs parallel to the steel beam and composite slabs with ribs transverse to the steel beam. The objectives of the study were to investigate the performance of headed studs for their capacity and failure modes at normal and elevated temperatures. An electric furnace was used and the temperature of the furnace was not heated according to the standard ISO

834 curve. The diameter of studs in the experiments was taken 19 mm with a height of 100 mm. The compressive strength of concrete after 28 days was 38.5 MPa. They concluded that the mode of failure for the solid slabs and composite slabs with ribs parallel to the steel beam was the shearing off of the headed studs. However, the mode of failure of the composite slabs with ribs transverse to the steel beam was a concrete crack failure but at high temperatures, it turned to be stud shear failure. Also, they pointed out that the formula in Eurocode 4 well-predicted the capacity of headed studs at elevated temperatures.
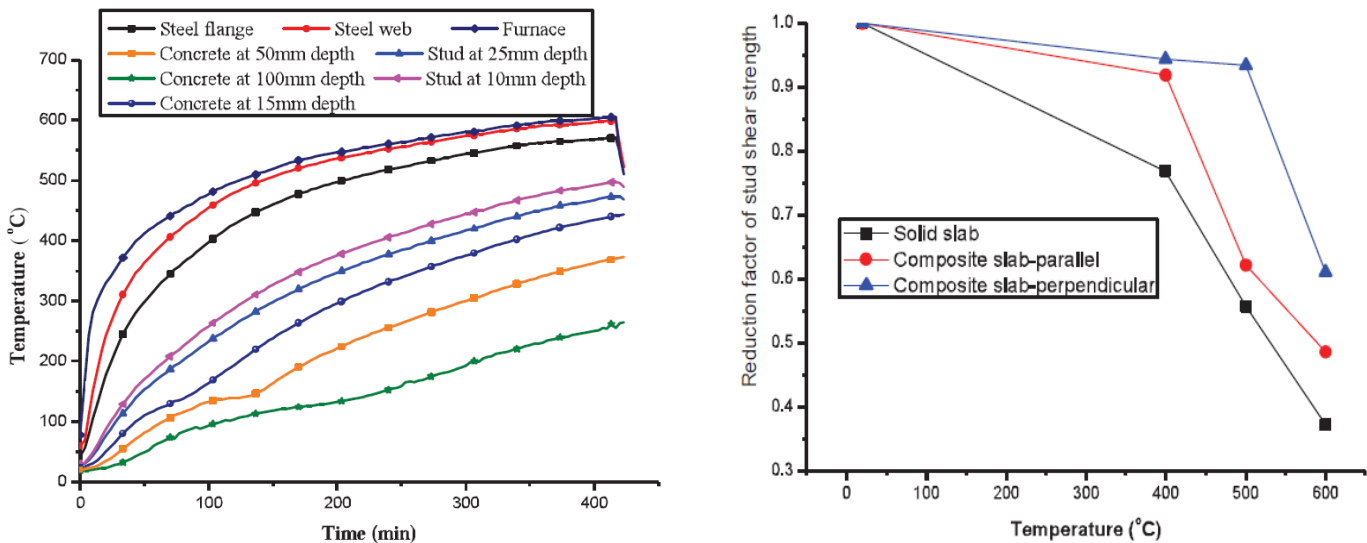
Fig. 17: Time-Temperature curve (left), Load-reduction factor curve (right) (Chen et al., 2015)

Chen et al. (2015) adopted the temperature of the stud at 10 mm from the flange of the steel beam as the temperature of the stud. The reason for this is because below the 10 mm, the thermocouples are mounted and they may cause some effects on the behaviour of the studs. Additionally, they made a comparison between existing test results by other researchers as shown in Fig. 18

Mirza, Uy and Krezo (2011) conducted push-out tests to investigate the behaviour of headed shear studs in solid and profiled slabs and to record the load-slip behaviour of studs at normal and elevated temperatures. The push-out tests were carried out at an ambient temperature, 200°C, 400 °C and 600°C. The experimental tests for the elevated temperatures

were heated according to the standard ISO 834 and they were based on the procedures according to Eurocode 4. The specimens were loaded with ratios from their ultimate capacity (40%) for 25 cycles before loading them to failure.
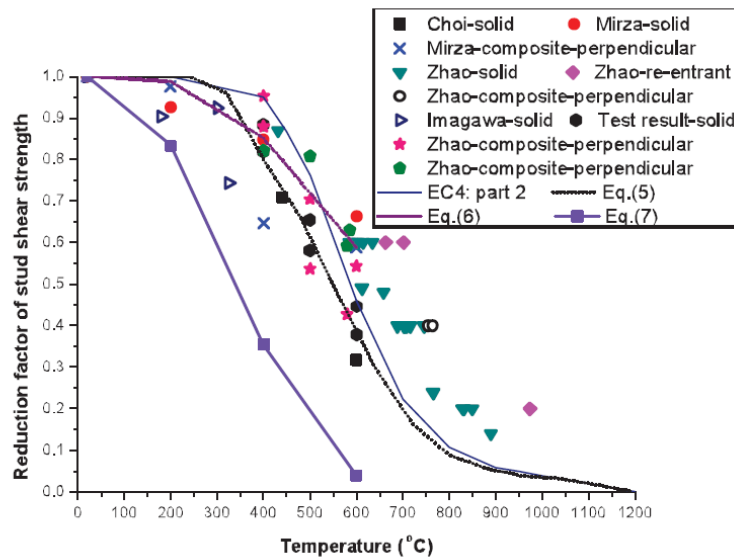
Fig. 18: Comparison between existing test results (Chen et al., 2015)

They concluded the following points:

- Shear connection failure of the headed shear studs with solid slabs
- The solid slabs accounted for higher ultimate loads than the profiled slabs
- The profiled slabs achieved more ductility than the solid slabs
- The profiled slabs showed a greater fire resistance compared to the solid slab as a function of their ambient temperature strength.
- It is argued by Hicks and Smith (2014) that the shear stud behaviour found in push tests may not be completely accurate to represent the actual shear stud behaviour in composite beams. This is due to the fact that there is no beam curvature that is caused by the floor loading resulting in a normal force unlike the push-out test. This has been concluded based on comparing the results between the full-scale composite beam tests with profiled steel sheeting and the push-out tests.

Fig. 19 : Headed stud shear failure at 200℃ (Mirza, Uy and Krezo, 2011)

Kruppa and Zhao (1996) established full-scale experiments on simply supported composite beams specified with different degrees of shear connections. The beams have a uniformly distributed load and tested under fire conditions. The specimens were exposed to the standard fire curve ISO 834 with and without applying fire protection. They concluded that for the case of an unprotected (fully composite) beam, the failure occurred in the shear studs. In the case of applying protection to the beams (partially composite), failure occurred in the shear studs as well due to the excess in the relative slippage between the concrete and steel which is initially caused by the difference in the thermal expansion between steel beam and concrete. The results from the full-scale tests are shown in Table 2

Table 2: Full-scale test results performed by (Kruppa and Zhao, 1996)

Dimensions of solid slab (mm)	Insulation thickness (mm)	Shear connection degree	Applied load (KN)	Fire resistance (min)	Failure mode
1200×120	0	100%	33.5	35	Plastification of steel section

800×120	25	100%	67.5	115	Mid-span concrete crushing at un exposed face
800×120	25	100%	102.5	70	Mid-span concrete crushing at un exposed face
1200×120	25	100%	102.5	76	Mid-span concrete crushing at un exposed face
1200×120	25	50%	79.5	68	Shear stud failure

Jiang et al. (2017) carried out two full-scale tests to evaluate the behaviour and design of composite beams with composite slabs at elevated temperatures. The composite beams were designed to have a full shear interaction. Furthermore, the composite beams were designed to be simply supported with steel sheeting parallel and transverse to the steel beam to represent the main and secondary beams supporting a typical slab of a building.
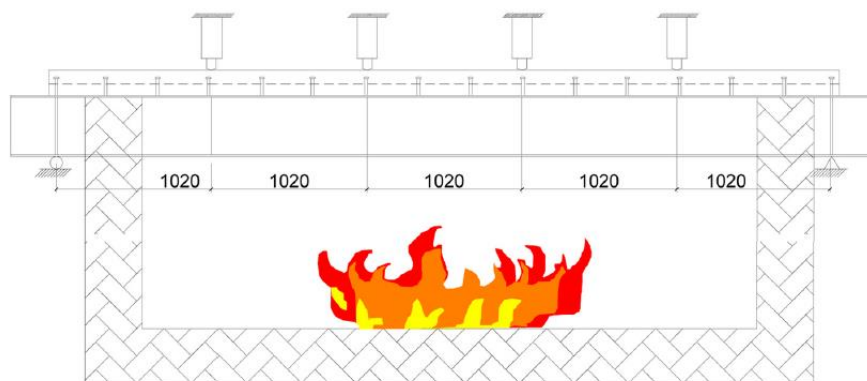
Fig. 20: test set-up for composite beam with composite slab at elevated temperatures (Jiang *et al.*, 2017)

A numerical model was established using ABAQUS software and the results were compared with the ones from the full-scale test. The composite beams are composed of a built-up I-section of steel plates with a span of 5.1 m to support a slab of 1.376 m width. The diameter of the headed studs used in the two specimens is 19 mm with a 120 mm height arranged with 300 mm spacing. The furnace was heated up according to the ISO 834 curve. The concrete compressive strength of the slab used was 33.3 MPa after 28 days. The maximum yield strength of the studs used was not specified and also there is no information regarding the built-up section whether it is welded or bolted. It was only mentioned that the steel section was fire protected with a certain thickness. They recorded the following failure observations with the two specimens: -

- Failure of both specimens due to large deformation and concrete crushing at the mid-span
- Spalling of fire protection at mid-span
- The bottom flange of the steel beam reached its yielding strength
- concrete cracking at the end of the slab in case of transverse sheeting to the steel beam
- Debonding of the concrete with the profiled sheeting at several locations for the 2 specimens

Despite carrying out a full-scale test, the authors did not point out any failure in the headed studs used in the composite slab which is questionable. They also concluded that the design predictions prescribed in Eurocode 4 are conservatively taken after comparing them with the results calculated from the numerical model and their experimental work.

It is seen that the researchers performed the push-out tests with various compressive strengths of the concrete slab. The values that have been used range from 35 to 40 MPa. Furthermore, the typical dimensions of shear studs used were 19 mm × 100 mm except the studs used during the tests by Imagawa et al (2012) which were 22 mm × 150 mm. The capacity of shear studs ranged from 102 to 127.6 kN for the 19 × 100 mm studs, while for
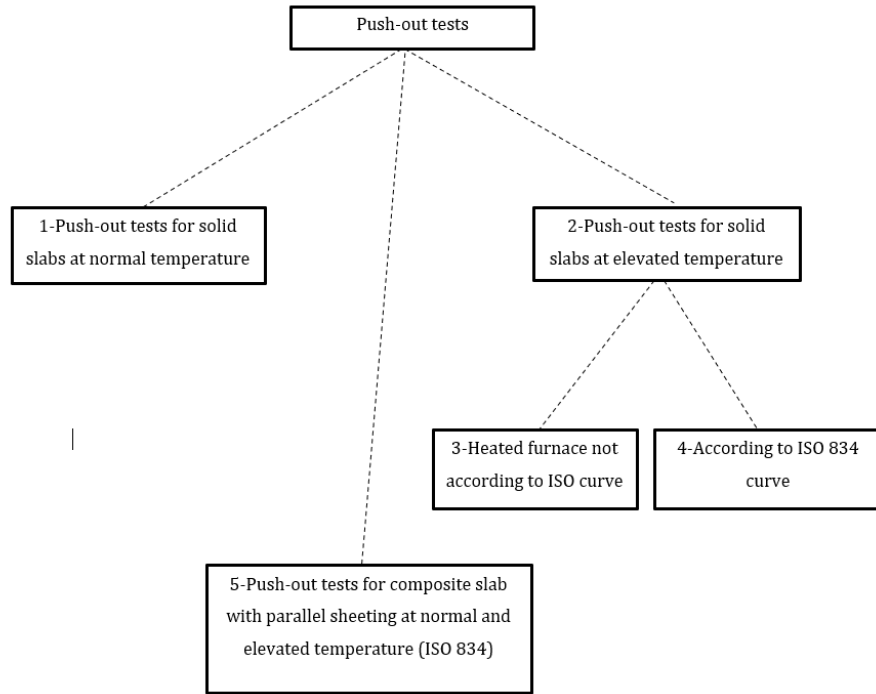
Fig. 21: Sequence of comparison between different push-out tests

Table 3:
Comparison between values of solid slab push-out tests at normal temperature

	Studs Dia×height (mm)	Stud's ultimate strength (MPa)	Concrete strength (MPa)	Average Stud's capacity of specimens (KN)
Lam and El lobody (2005)	19×100	F_y=470.8	35	102
Chen et al. (2015)	19×100	Not defined	38.5	127.6
Choi et al. (2009)	19×100	427	30	120
Imagawa et al. (2012)	22×150	400	32×1.25=40	160

the 22 × 150 mm studs the average capacity of specimens used reached up to 160 KN. The capacity of the stud with 22 ×150 mm dimensions accounted for higher value which is reasonable as the shear strength of the stud is directly proportional to square of the shank diameter according to Eq. (1) or Eq. (2) From Eurocode 4.

To conclude the performance of studs in solid slabs at normal temperatures, it has been shown by different push-out tests that the headed stud shank rupture is always the case of failure. Only concrete failure was observed for low (20 MPa) and medium concrete strength (30 and 35 MPa) in the push-out tests performed by Lam and El-Lobody (2005)

Table 4: Comparison between values of solid slab push-out tests at elevated temperature with the heated furnace not according to ISO 834 curve

	Heating condition	Studs Dia×height (mm)	Stud's ultimate strength (MPa)	Concrete strength (MPa)	Average Stud's capacity of specimens (KN)
Chen et al. (2015)	Up to 500°C	19×100	Not defined	38.5	71.2
Imagawa et al. (2012)	up to 500°C	22×150	400	32×1.25= 40	148
Imagawa et al. (2012)	up to 300°C	22×150	400	32×1.25= 40	144

Comparing the results of Chen et al. (2015) and Imagawa et al. (2012) who performed push-out tests at elevated temperatures with a heated furnace not according to ISO 834. The failure always occurred in the headed shear studs. Results of the headed studs' capacities were recorded by both at 500°C. Chen et al. (2015) found that the stud's capacity efficiency was 55.8 % only compared to their tests at normal temperature. On the other hand, Imagawa et al. (2012) reported a pleasant capacity of 92.5 % compared to their tests at the normal temperature as the strength of concrete used was slightly higher than the one in Chen et al. (2015) experiment. This capacity is doubtful since it should be less than the recorded

capacity at 300°C at the same elevated test, which was 90 % of the value at normal temperature, taking into account that the dimensions of the studs used are 22 mm × 150 mm.

Table 5: Comparison between values of solid slab push-out tests at elevated temperature with heated furnace according to ISO 834

	Heating condition	Studs Dia×height (mm)	Stud's ultimate strength (MPa)	Concrete strength (MPa)	Average Stud's capacity of specimens (KN)
Choi et al. (2009)	500°C	19×100	427	30	85
Choi et al. (2009)	700°C	19×100	427	30	38
Mirza (2011)	400°C	Not defined	Not defined	Not defined	108
Mirza (2011)	600°C	Not defined	Not defined	Not defined	84.5

Analysing the outcomes of Choi et al. (2009) and Mirza (2011) whose experiments were conducted according to the ISO curve 834. It has been proven that the shear studs shank failure is the predominant mode of failure. Regarding the strength of the studs after 30 and 60 minutes, Choi et al. (2009) recorded a capacity of 70.83 % of initial strength at normal temperature after 30 minutes which decreased to 31.6 % after 60 minutes. The temperature that was reached after 30 and 60 minutes was 500°C and 700°C respectively at the base of the stud. On the other end, Mirza (2011) recorded a higher strength of shear studs at 100°C lower temperatures. A capacity of 84.7 % of ambient temperature strength was achieved at 400°C which is then reduced to 66.3 % after temperature reached 600°C. This difference in capacities is reasonable since Choi et al. (2009) recorded the strength at higher temperatures than Mirza (2011). It is worth mentioning that Choi et al. (2009) obtained the ultimate capacity of the studs at a slip of 5 mm while Mirza (2011) at 4 mm.

Table 6: Results of the push-out tests of the composite slab with parallel sheeting at normal and elevated temperatures

	Heating condition	Studs Dia×height (mm)	Stud's ultimate strength (MPa)	Concrete strength (MPa)	Average Stud's capacity of specimens (KN)
Chen et al. (2015)	20°C	19×100	Not defined	38.5	100.25
Chen et al. (2015)	600°C	19×100	Not defined	38.5	48.5
Chen et al. (2016)	20°C	19×100	475	35.1	99.75
Chen et al. (2016)	600°C	19×100	475	35.1	55.68

Table 6 illustrates the comparable results recorded by Chen et al. (2015) and Chen et al. (2016). The same dimensions of studs were used (19 mm × 100 mm) and a quite similar concrete compressive strength. The rate of rising in temperature in the experiments by Chen et al. (2016) was smaller than the standard ISO 834 curve, however, no significant variations in temperatures at 5 mm from the base of the stud were observed. It is seen that at normal temperature for both tests, almost the same capacity of the stud was recorded with a negligible difference. Nevertheless, at elevated temperatures (600°C), Chen et al. (2016) achieved a higher capacity with nearly 4 % more. Regarding the failure modes for Chen et al. (2015), stud failure accompanied by the separation between the deck and concrete took place at normal temperature and stud failure only at elevated temperature. Chen et al. (2015) mode of failure is a stud failure accompanied with a concrete shear failure at ambient temperature. At elevated temperature, stud shearing off occurred.

Comparison between the two full-scale tests by Kruppa and Zhao (1996) and Jiang et al. (2017)

Even though the experiments performed by Kruppa and Zhao (1996) and Jiang et al. (2017) were performed on different types of slabs (solid and composite) and different degrees of shear connection, a direct comparison can be made between the results of both tests. For the case of applying fire protection to the beams, concrete crushing was always observed at the mid-span for both tests and accompanied by spalling of the fire protection in Jiang et al. (2017) test. In the case of an unprotected fully composite beam by Kruppa and Zhao (1996), they found that it is not likely to fail due to the failure of the shear studs but rather steel section plastification occurred. Shear stud failure was only recorded in the case of protected beams with 50% shear connection. On the other hand, Jiang et al. (2017) did not identify any failure to the headed studs used in the composite slab.

Performing full-scale experimental tests for composite beams is a time-consuming and costly option. Besides, such tests require a large space in the research labs. Instead, finite element (FE) simulations are encouraged to replace most of the experiments with accurate models that can predict the non-linear behaviour of materials.

1.8 Objectives of the thesis

This thesis is mainly focused on developing a three-dimensional finite element model for investigating the mechanical behaviour of the headed shear stud in solid and composite slab. This is achieved through development of the load-slip curves through using the appropriate non-linear material models along with the best analysis approach to get comparable results with the experimental or numerical results of other researchers. The objectives are arranged in the following order:

- Capture the predicted failure mode at normal temperature for solid and composite slab.
- Compare the shear stud strength with the Eurocode 4 provisions.

- Develop a steady-state heat transfer model with temperature dependent material properties to have a considerable thermal gradient within the solid concrete slab.

- Create a thermo-mechanical analysis with the reduction in the non-linear material properties of concrete and steel to evaluate the difference in the load-slip behaviour at elevated temperatures for solid slab.

- Perform a parametric study to assess the difference in the performance of the headed shear stud by changing some model parameters and the dimensions of the stud as well.

The commercial software ABAQUS was chosen to carry out the numerical modelling because of its ability to simulate the complexity of the non-linear performance of real-world applications. Regarding the contact between different elements, its graphical user interface simply provides several forms of materials contact to represent real-life scenarios. By far, the contact results with different surfaces were reputable with their accuracy. Also, it has the capability to perform a thermo-mechanical analysis simultaneously in one simulation, unlike other programs that have to do it separately. Concerning damage and failure, ABAQUS has a framework that simulates damage initiation and evolution for bulk material failure over a wide range of materials such as concrete, metals and composites.

ABAQUS FE software performs the stress analysis using the Von Mises failure theory which is commonly the case in FE software. The equivalent Von Mises stress is a common output from the stress analysis performed by the software. If the equivalent Von Mises stress is larger than the yield strength of the material, yielding is predicted to occur. This is typically presented in the FE analysis results inform of contours to demonstrate the distribution of the Von Mises equivalent stress in an element. These contours enable the identification of prone areas of yielding.

ABAQUS/Explicit is considered to be more applicable than ABAQUS /Standard for this type of analysis as ABAQUS/Standard will not be able to solve the damage problem where a material degradation and crack propagation takes place. Also, ABAQUS/Explicit is better due to the complexity in the contact interaction between the steel metal sheeting, concrete, stud and the steel beam section. In addition, the dynamic explicit analysis is unlike the static

analysis as it does not experience the convergence problems that arise due to material damage and failure. For this type of explicit solver, the unknown values at a later time are computed using the already known values at the current time. On the other hand, for the standard analysis, an equation has to be solved which is function of the current and later time to get the unknown values at a later time.

2. Methodology for the numerical modelling

2.1 Model setup and overview

A schematic diagram as shown in Fig. 22 was developed to track the FE model approach. This chart demonstrates the sequence of the approach for the solid and composite slab that was taken. In addition, a summary of the entire modelling technique for all the FE analyses was provided in Table 7.
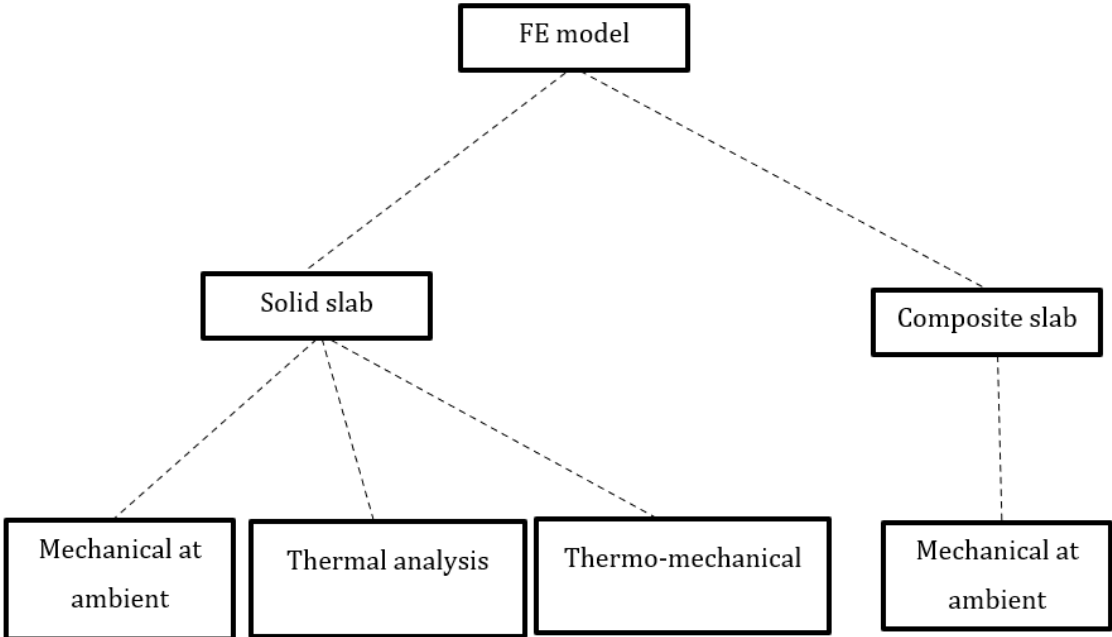
Fig. 22: Sequence of the FE model approach for push-out tests

Table 7: Summary of the modelling technique for all the FE analyses

	Solid slab	Composite slab	Thermal analysis (solid slab)	Thermo-mechanical (solid slab)
Analysis type	ABAQUS/Explicit	ABAQUS/Explicit	ABAQUS/Standard	ABAQUS/Explicit
Block dimensions	300 mm × 120 mm	213 mm × 145 mm ×76 mm × 1.2mm	300 mm × 120 mm	300 mm × 120 mm
Stud dimensions	19 mm × 100 mm	19 mm × 100 mm	19 mm × 100 mm	19 mm × 100 mm
Concrete model	Concrete damaged plasticity	Concrete damaged plasticity	N/A	Concrete damaged plasticity
Damage parameters	Yes	Yes	N/A	No
Steel properties	Perfect-plastic F_y=470.8 MPa	Perfect-plastic F_y=470.8 MPa	Thermal temperature dependant properties (EC4)	Mechanical properties at elevated temperatures (EC4)
Concrete properties	F_{ck} =30 MPa	F_{ck} =30 MPa	Temperature dependant properties (EC4)	Mechanical properties at elevated temperatures (EC4)
Boundary conditions	ENCASTRE at block base + Z SYMM at other end	ENCASTRE at block base + Z SYMM at other end	Temperature conditions (Kruppa ,1996)	ENCASTRE at block base + Z SYMM at other end
Element type	3D stress (C3D8R)	3D stress (C3D8R)	Heat transfer (DC3D20)	3D stress (C3D8R)
Loading rate	Velocity 0.5 mm/s	Velocity 0.5 mm/s	N/A	Velocity 0.5 mm/s
Interaction	Stud embedded in concrete	Stud embedded in concrete + contact between sheeting, concrete and flange	Stud embedded in concrete	Stud embedded in concrete

2.1.1 Solid slab

The part module in ABAQUS was used to establish the geometry of the push-out test as illustrated in Fig. 23. The configuration of the test consists of a concrete block which resembles the solid slab of dimensions 250 mm × 300 mm with a thickness of 120 mm. The concrete block is connected to a steel flange (150 mm × 250 mm × 10.7 mm) of an IPE 300 through headed shear studs of dimensions 19 mm ×100 mm. The head of the stud has a diameter of 30 mm and thickness of 10 mm. The total height of the stud is 95 mm without the weld collar. The Stud and steel flange were firstly created separately and then the bottom surface of the stud was merged together with the corresponding surface of the top steel flange to simulate the weld at the assembly module. The steel mesh was not modelled in this numerical test because it was considered to be unnecessary since the concrete damaged plasticity model for concrete can be used for plain or reinforced concrete.
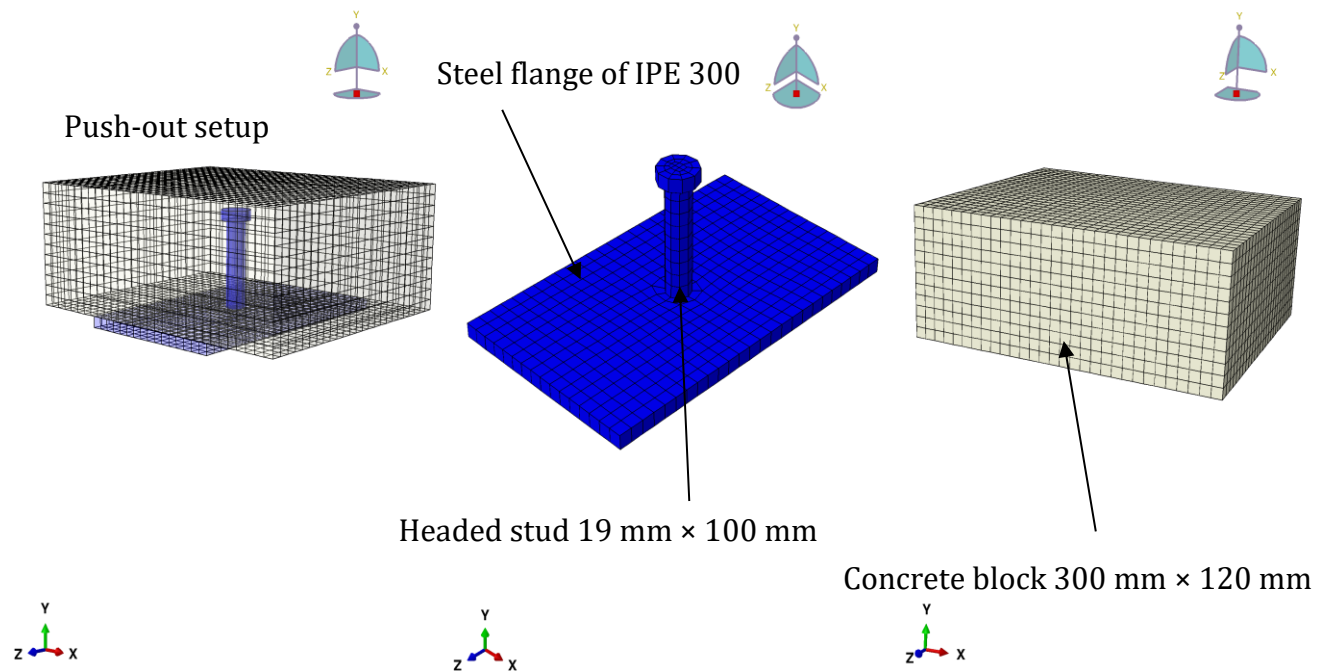
Fig. 23: Setup of the finite element push-out test of solid slab

2.1.2 Composite slab

Similarly, as in the solid slab, the configuration of the composite slab test consists of a steel flange of IPE 300 connected to a trapezoidal concrete block through headed shear studs (19 × 100 mm) welded through the deck. The profiled steel sheeting has a thickness of 1.2 mm and the trough is fixed parallel to the steel flange. Each of the concrete block, the profiled sheeting and steel flange were created separately in the parts module and assembled to form a complete model of the profiled slab. The Stud and the steel flange were merged together. Then, this merged part was attached to the trapezoidal concrete block and the metal steel sheeting in the assembly module. The cross-section of the corrugated sheet used was similar to the one used by Chen et al. (2016) in their experiments.
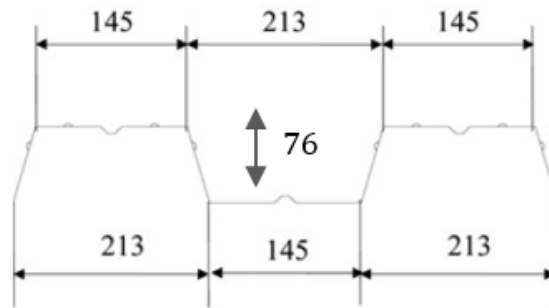
Fig. 24: cross-section of the corrugated sheet (Chen et al.,2016)

2.2 Finite element type and meshing

The different components comprising the concrete slab, headed shear stud and steel flange were modelled using the reduced integration three-dimensional continuum eight-node solid brick elements (C3D8R). The reason for choosing the reduced integration brick elements is because of their reasonable accurate solution with less computing time compared to other types of elements. This has been proven by running some simulations using the (C3D8) solid brick elements. In addition, the ABAQUS/Explicit option has been chosen for the element library with linear geometric order. For establishing the mesh, the merged part of the stud and the flange were partitioned at the tip of the stud head so that they can be meshed using the sweep technique. Each of the concrete block and the merged part were allowed to be independent for the sake of meshing the whole model together with global size seeding of

10. In the case of the composite slab, the same elements were used, but only the profiled steel sheeting was modelled with the four-node doubly curved shell elements (S4R).

Push-out setup

Corrugated sheet

Trapezoidal block

Steel flange of IPE 300   Headed stud 19 mm ×100 mm
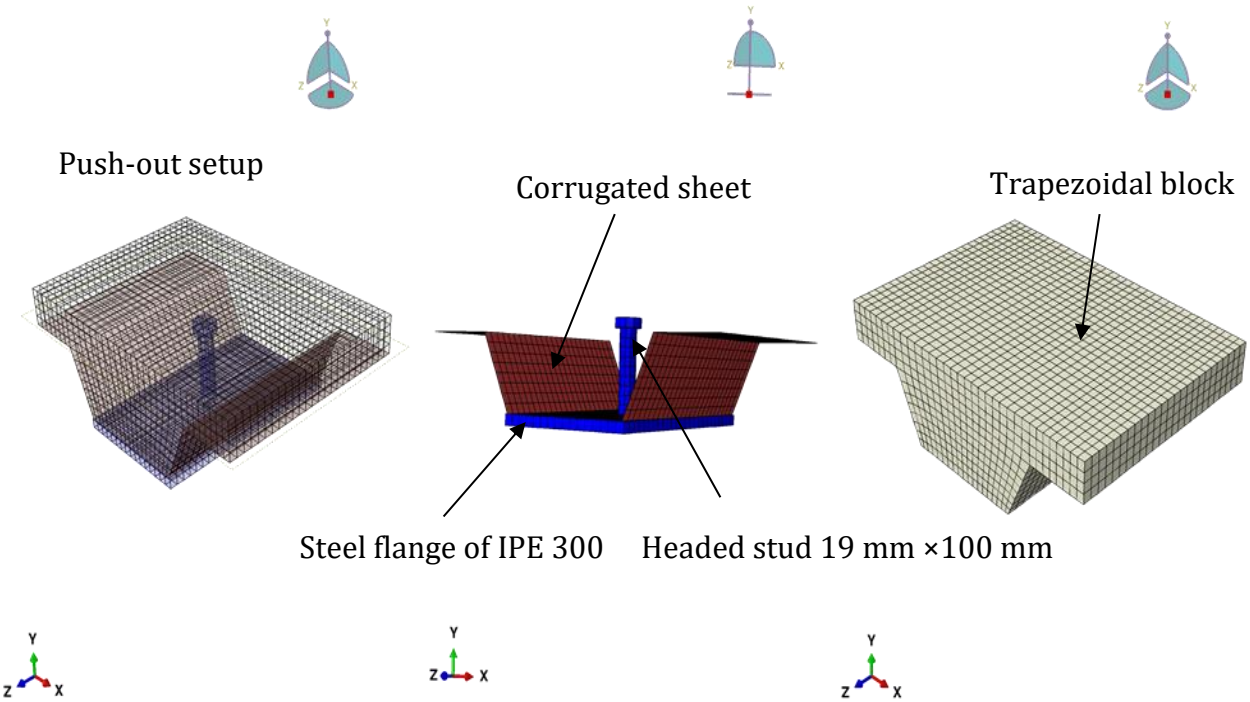
Fig. 25: setup of the finite element push-out test of composite slab
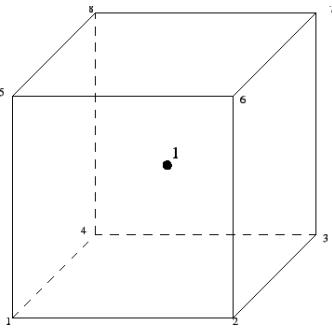
Fig. 26: C3D8R element type used for the solid elements (ABAQUS documentation)

2.3   Boundary conditions and loading

To simulate the experiment of the push-out test, the base of the concrete block indicated as (surface 1) is restricted from either moving or rotating in all directions using the ENCASTRE boundary condition. Regarding the IPE steel flange, it is restricted from any displacement in the X and Y direction. The load applied is in the form of a uniform velocity with rate 0.5 mm/s using a smooth amplitude along the longitudinal Z axis of the flange pointed out (surface 2) as shown in Fig. 27. A smooth-amplitude was chosen for applying the velocity as instantaneous loading may induce the propagation of a stress wave through the model, producing undesired results. This has been done to ensure a quasi-static solution. For the other end of the slab (surface 3), "ZSYMM" boundary condition was applied to account for the continuity of the slab in the Z direction. The same approach was followed in the composite slab.

ENCASTRE
surface 1

Loading
surface 2

ZSYMM
surface 3
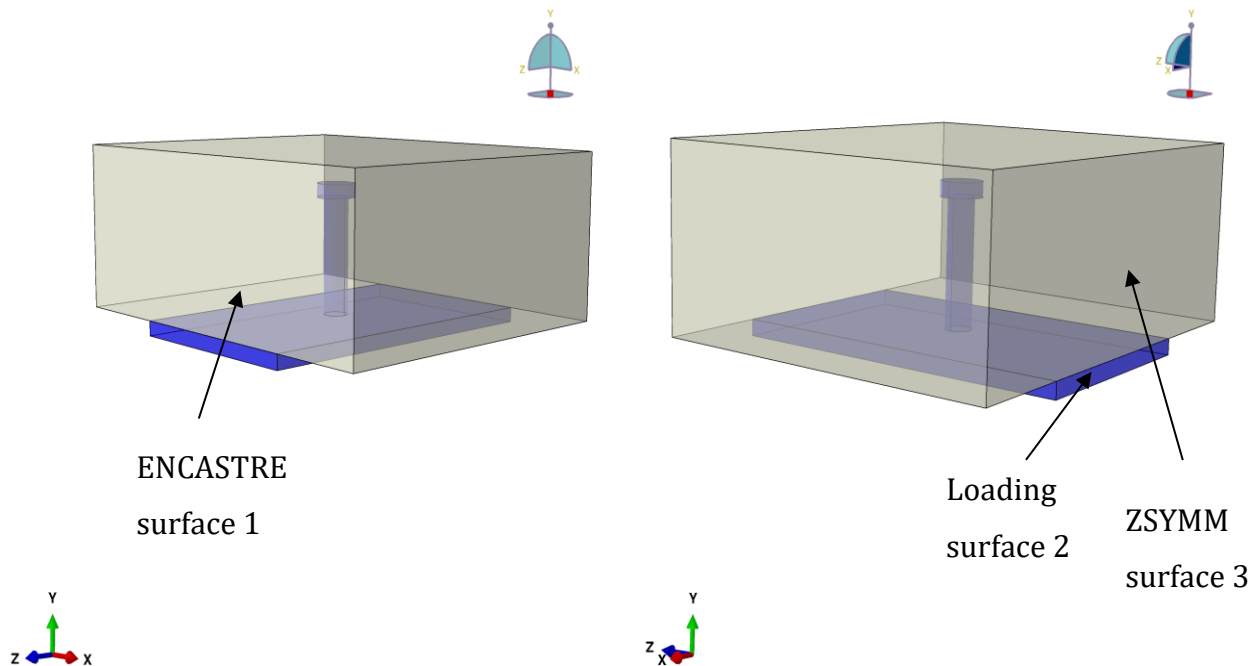
Fig. 27: Boundary conditions and loading surface

2.4   Constraints and contact interactions

The interaction between different components is negotiated to be the challenging part of the simulation. This is due to the complexity of the composite geometry. The surface interactions need to be defined properly to simulate the real push-out test. Firstly, the attachment of the shear stud to steel flange to simulate the weld collar. This has been done by merging the two parts together as mentioned earlier. Similar approach was followed in the finite element modelling of steel-concrete composite beams done by Katwal et al. (2018). Regarding the interaction between the headed shear stud and concrete block, the embedded constraint was used where the stud acted as the embedded region and the concrete block as the host region. The same strategy is used to represent the reinforcing bars for the finite element modelling of reinforced concrete beams or slabs. Since the steel flanges are usually greased during the push-out experimental tests to prevent the bond between the slab and the steel before the concrete cast, no interaction has been defined between the concrete block and the steel flange in this finite element model.

In case of composite slab, the interaction property between concrete and the profiled steel sheeting, was defined using the surface-to-surface contact algorithm. The tangential and normal behaviour to the surfaces were defined. The tangential behaviour was defined with a penalty friction formulation and Eurocode 4 "section 6.7.4.2" assumed a value 0.5 for the coefficient of friction between the concrete slab and the steel metal deck. The contact property of the normal behaviour was defined using the default Pressure-overclosure option "Hard" contact as this type enables a minimum penetration of a slave surface into a master surface.

The surface-to-surface contact algorithm works by defining the master and the slave surfaces. Typically, the stiffness of the material is the main key that drives the choice of which material should be assigned as the master surface. Materials of higher rigidity are usually assigned to be the master surface. For the concrete and corrugated sheet contact, the concrete surface was chosen as the master and the sheet as the slave. Regarding the contact between profiled steel sheeting and steel flange, it was implemented using the general

contact with a friction formulation "frictionless" for the tangential behaviour and Normal behaviour with "Hard" contact.

With respect to the interaction between the stud and metal sheeting, the tie constraint was used such that the base of the stud was tied to the upper surface of the steel metal sheeting.

2.5   Material model of steel

The design values of the material properties and coefficients for structural steel were taken according to the specifications of EN1993-1-1. The modulus of elasticity (E) was taken as 210 GPa. The ratio of Poisson in elastic range (ν) has a value of 0.30. The steel used in the model for the headed stud and steel flange was adopted from Lam and El-lobody (2005). The average of the three coupons tested in their experiments was 470.8 N/mm^2. It is considered to be linear elastic until the yielding point F_y=470.8 N/mm^2. Then, the steel behaved as a perfect plastic material. The elastic-plastic bilinear stress-strain curve is inputted in the model as shown in Fig. 28.

Table 8: Summary of the steel material properties used for all steel elements

Material	Property	value	Unit
Steel	Density	7.95×10^{-9}	ton/mm^3
	Poisson's ratio	0.3	None
	Modulus of elasticity	210	GPa
	Yield strength	470.8	MPa
	Yield strain	2.24×10^{-3}	mm/mm

2.6   Concrete material model

There are many modelling methodologies available in the ABAQUS library to simulate the behaviour of concrete in tension and compression such as Concrete Smeared Cracking, Brittle Cracking, Drucker-Prager Hardening and Concrete Damage Plasticity (CDP). In this model, the CDP model for concrete was adopted.
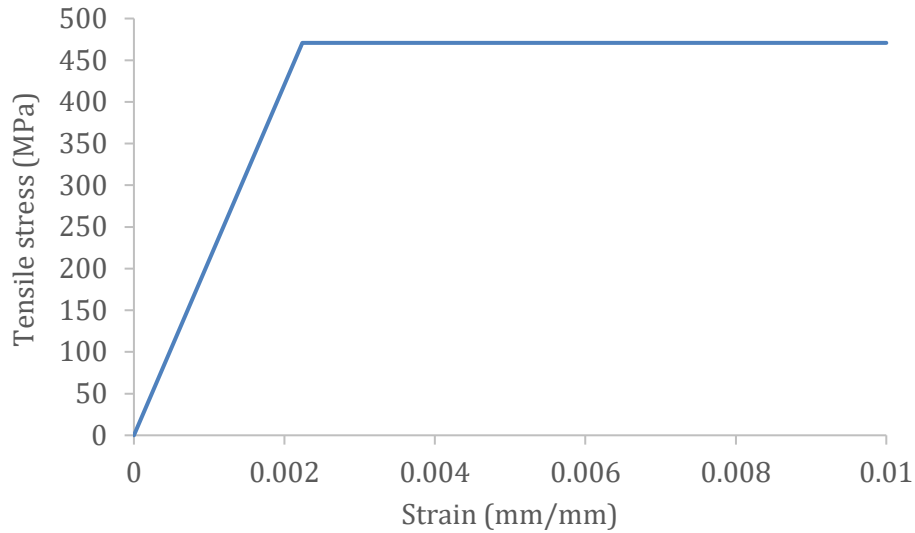
Fig. 28: Uniaxial stress-strain curve of structural steel

Table 9: properties of concrete material used in the FE model

Property	value	Unit
Density	2.6455×10^{-9}	ton/mm^3
Modulus of elasticity	24663.4	MPa
Poisson's ratio	0.2	none
f_{ck} of concrete (cylinder)	30	MPa

2.6.1 Concrete Damaged Plasticity Model (CDP)

The concrete damaged plasticity model in ABAQUS is used to model the inelastic behaviour of concrete as this model focuses on the concrete isotropic compressive crushing failure of the slab and the tensile cracking. It was found by Lam and Qureshi (2010) that the CDP model well-predicted the capacity of the studs, the load-slip behaviour and the failure mode of shear connectors with profiled steel sheeting. In the FE analysis where significant plastic deformation takes place, the true stress-strain curves are essential to be used instead of the engineering stress-strain curves. Consequently, it is necessary to define the true stress-strain curve for concrete in compression in the model as well as the stress-strain curve for concrete in tension.

2.6.2 Compression behaviour of concrete

The plain concrete behaviour has been adopted according to Carreira and Chu (1985) who proposed a general form of the serpentine curve to describe the complete stress-strain relationship of plain concrete in compression. It has been an issue to find a general stress-strain formula with parameters that are not dependant on the testing conditions.

They proposed the following equation: -

$$f_c = \frac{f_{cm}\ \beta\ (\frac{\varepsilon}{\varepsilon_{co}})}{\beta - 1 + (\frac{\varepsilon}{\varepsilon_{co}})^\beta} \qquad \text{Eq. (13)}$$

where, f_c is the compressive stress in concrete (MPa); ε is the strain in concrete; f_{cm} is the maximum stress (mean concrete compressive strength) (MPa); ε_{co} is the strain at ultimate stress and β is defined as:

$$\beta = \left(\frac{f_{cm}}{32.4}\right)^3 + 1.55 \qquad \text{Eq. (14)}$$

The strain at the maximum stress ε_{co} was taken as 0.0022 according to Table 3.1 in "EN 1992-1-1" and the ultimate nominal strain was calculated until 0.014. The descending branch of the stress-strain relation is then computed by multiplying the coefficient β by a value of 1.25 after trials which proved to give consistent results for the post-beak branch (Thoronfeldt et al.,1987). The in-elastic strain is then calculated by subtracting the total strain from the ratio between the stress and the elastic modulus.

2.6.3 Damage of concrete in compression

To define the crushing behaviour of concrete in compression, the compressive damage variable (d_c) versus the inelastic strain curve is developed using the following two equations:

$$d_c = 1 - \left(\frac{f_c \, E^{-1}}{\varepsilon^{\sim pl} \left(\frac{1}{b_c} - 1 \right) + f_c \, E^{-1}} \right)$$

Eq. (15)
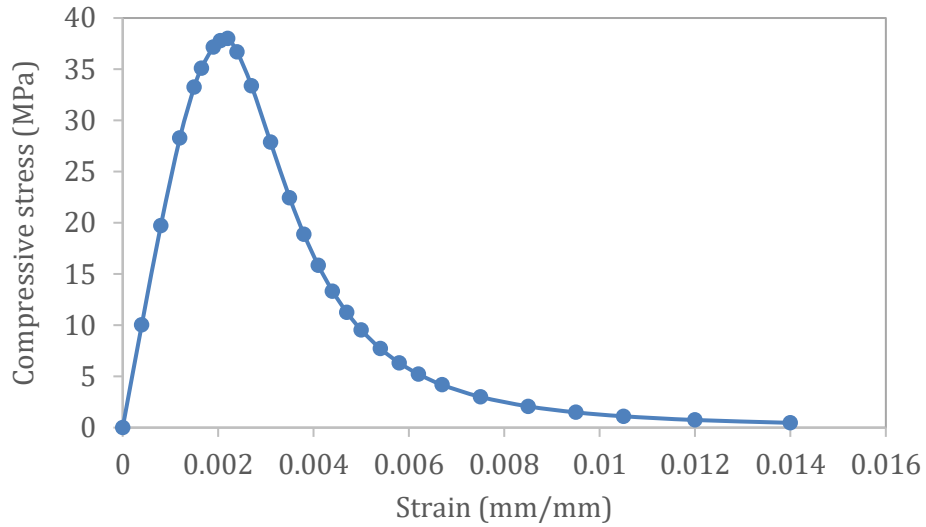
Fig. 29: Engineering compressive stress-strain curve for concrete using Eq. (13) and Eq. (14)
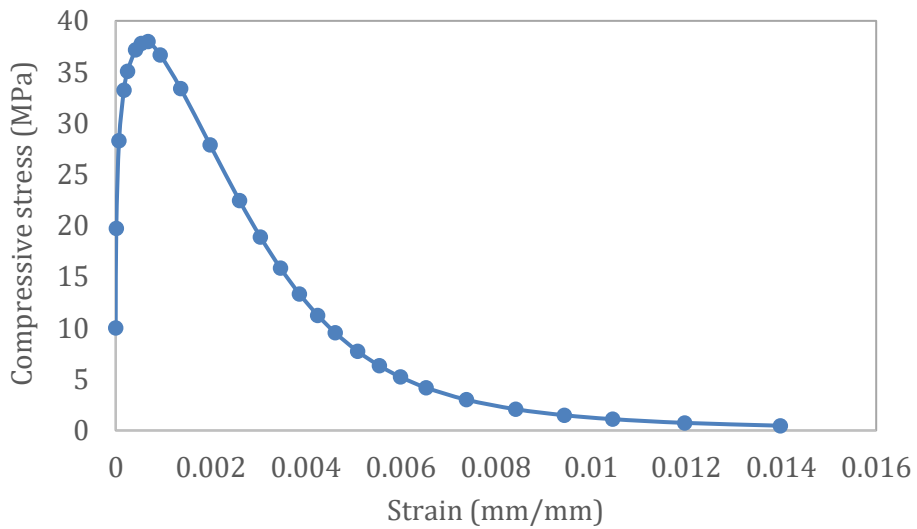
Fig. 30: True plastic compressive stress-stain curve for concrete

$$\varepsilon^{\sim pl} = b_c \times \varepsilon^{\sim in}$$

<div align="right">Eq. (16)</div>

Where, $\varepsilon^{\sim in}$ is the compressive inelastic strain, $\varepsilon^{\sim pl}$ is the compressive plastic strain and E is considered the elastic stiffness of undamaged concrete. The coefficient b_c has values between 0 and 1. A suggested value of $b_c = 0.7$ is taken according to the simulations done by Birtel and Mark (2006) for a FE model of a reinforced concrete beam. If the damage variable is zero, that means the concrete is undamaged, and a value of 1 stand for complete damage. The compressive damage values should always be ascending as the stress increases and should not comprise negative values to avoid errors before running the simulation.
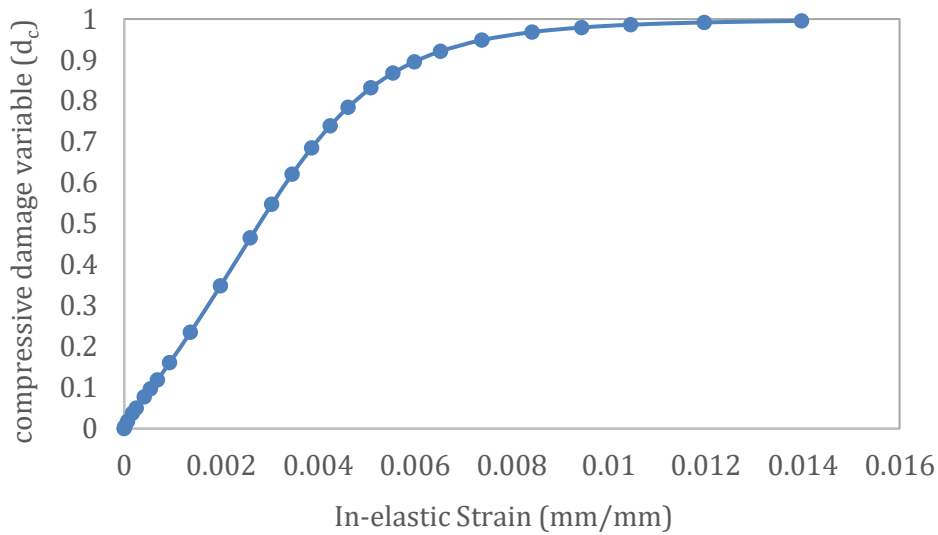
Fig. 31: compressive damage versus in-elastic strain curve

2.6.4 Plasticity Parameters of CDP model

Concrete exhibits a significant volume change when it is subjected to severe inelastic stress. This is typically referred to as dilation which could be defined by a proper plastic function, unlike the yield surface which could be defined by the hardening rule. Several parameters are needed to be defined in this model such as the dilation angle, eccentricity, ratio of

compressive strength under biaxial loading to uniaxial compressive strength (f_{b0}/f_{c0}), ratio of the second stress invariant on the tensile meridian to that on the compressive meridian (K) and the viscosity parameter. The value of the dilation angle is entered in degrees. The eccentricity is a small positive number that defines the rate at which the hyperbolic flow potential approaches its asymptote. For the K value, at initial yield for any given value of the pressure invariant p such that the maximum principal stress is negative, $\sigma_{max} < 0$. It must satisfy the condition 0.5 < Kc <1.0. Regarding the viscosity parameter, it is used for the visco-plastic regularization of the concrete constitutive equations in ABAQUS/Standard analyses. This parameter is ignored in ABAQUS/Explicit. The default values were used for the plasticity parameters except the dilation angle was assumed 15° (ABAQUS documentation). The values of the plasticity parameters are mentioned in Table 10.

Table 10: Plasticity parameters for concrete damaged plasticity model

Dilation angle(ψ)	Eccentricity (e)	f_{b0}/f_{c0}	Kc	viscosity parameter
15°	0.1	1.16	0.666	0

2.6.5 Tensile behaviour of concrete

The uniaxial tensile behaviour of concrete in ABAQUS can be simulated either by using the stress-strain relationship in tension or by using the fracture energy. The latter describes the softening behaviour of concrete in terms of crack displacement. As a result of the localized cracking, the descending part of the stress-strain curve cannot be a material property such as the elastic modulus. This softening response is defined by various ways. Instead of using the normal stress-strain curve to simulate the tensile behaviour of concrete, the fracture energy is used which is an appropriate approach to model cases with unreinforced or little reinforcement like the case for this push-out test. This tension stiffening approach expresses the brittle failure of concrete in tension. The fracture energy (G_f) is defined by Hillerborg et al. (1976) to be the energy needed to form a unit area of a crack. This is typically represented

by the area under the stress-crack opening curve (the area under the unloading part) for a given concrete strength (ABAQUS documentation).

Qureshi and Lam (2012) managed to establish a successful model with an exponential function to represent the softening behaviour of concrete in tension which was primarily developed by Cornelissen et al. (1986). Reasonably realistic results have been obtained by this exponential expression to study the post-failure tensile behaviour of concrete.
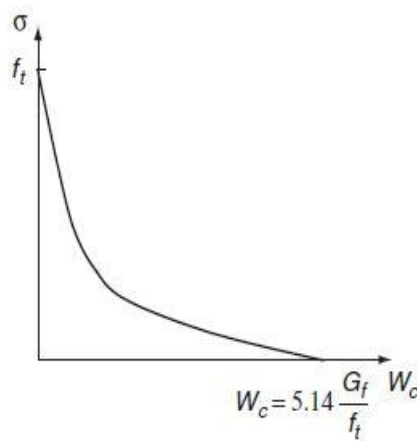
Fig. 32: Exponential function for tension softening model (Cornelissen et al., 1986)

The softening curve for the tensile stress and the cracking displacement can be developed using Eq. (17). The axial tensile strength of the concrete is calculated using "EN 1992-1-1" provisions and it is multiplied by a dynamic amplification factor of 1.1 to account for the rate effects.

$$\sigma_t = f_t \left\{ f\left(w\right) - \frac{w}{w_c} f\left(w_c\right) \right\}$$

Eq. (17)

$$w_c = 5.14 \left(\frac{G_f}{f_t} \right)$$

Eq. (18)

where, w = the crack opening displacement; w_c = the ultimate crack opening displacement; c_1 and c_2 are material constants and can be taken 3.0 and 6.93 respectively for normal density concrete.

The fracture energy was calculated from the following equation as per the design code MC 10 CEB-FIP (2010)

$$G_f = G_{fo} \left(\frac{f_{cm}}{f_{cmo}}\right)^{0.7}$$
Eq. (19)

where, f_{cmo} represents the base value of mean compressive cylinder strength with a value equal to 10.

G_{fo} is obtained from Table 11, and it is the base value of the fracture energy and depends on the maximum aggregate size.

Table 11 : Base values of fracture energy G_{fo} with different aggregate sizes (MC 10 CEB-FIP, 2010)

d_{max} (mm)	G_{fo} (Nmm/mm2)
8	0.025
16	0.030
32	0.058

Eventually, the tensile damage of concrete could be calculated based on the values of the tensile stress and the concrete ultimate tensile stress from the following equation:

$$d_t = \left(1 - \frac{\sigma_t}{f_t}\right)$$
Eq. (20)

The tensile damage values versus the cracking displacement for the characteristic compressive strength of 30 MPa is illustrated in Fig. 34.
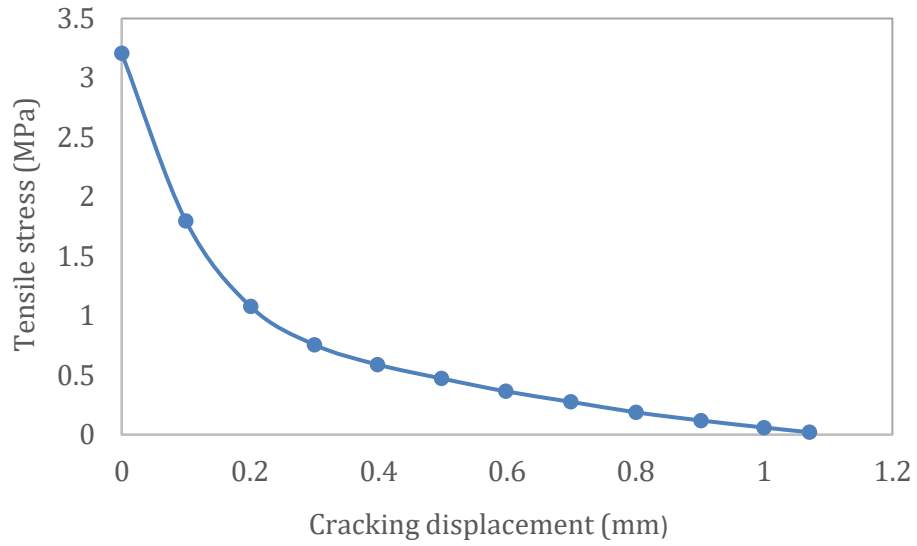
Fig. 33: Tensile stress versus cracking displacement curve
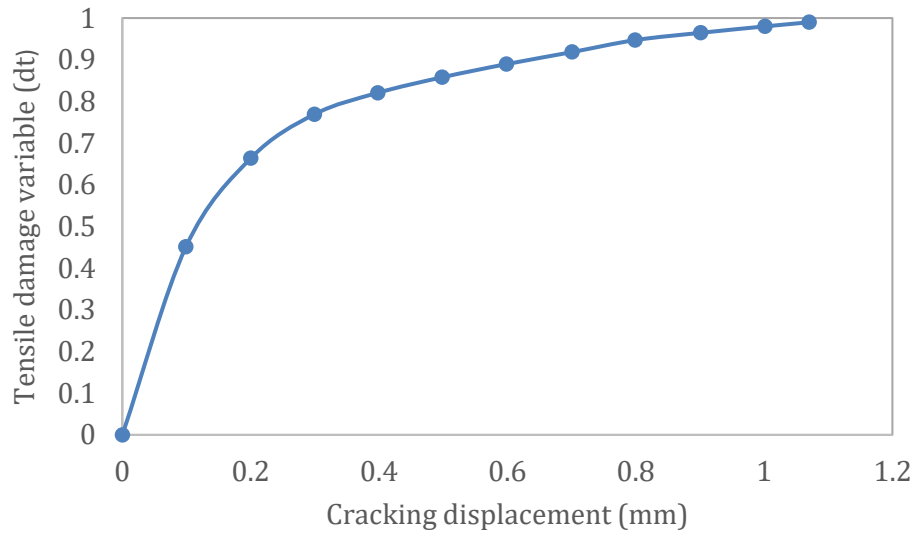
Fig. 34: Tensile damage versus cracking displacement curve

2.7 Analysis procedures

For this FE model of the push-out test, a quasi-static solution is required to be performed using the ABAQUS/Explicit solver by applying the load slowly using a uniform velocity with a smooth-amplitude function. This should be done with care because if the load is applied with a fast rate, the dynamic effects inform of inertia will start to play a significant role in the solution and will drastically influence the results. Generally, in explicit analyses, the simulation time could be reduced by applying the load faster. Nevertheless, for reducing the dynamic effects, another approach is used which is by introducing the mass scaling in the step module to decrease the simulation time. By increasing the mass, the stable time increment can be increased leading to a shorter simulation time.

The solution for the quasi-static analysis that is done in a natural time-scale should be comparable to the static solution. For this reason, and to determine the appropriate loading rate for the push-out test, a series of analyses were conducted with various loading rates and mass scaling. Many trials were performed with different loading rate and mass scaling factor of 10, 100, 100, 1000 and 10,000. It is important to ensure that the ratio between the kinetic to the internal energy (ALLKE/ALLIE) of the system do not exceed a fraction between 5 to 10 % throughout most of the simulation. As above this limit, the inertia effects will start to influence the results as per recommendation of the ABAQUS manual.

A mass scaling factor of 10 along with a loading rate of 0.5 mm/s and mesh size of 10 mm × 10 mm were proved to be reasonable to achieve a quasi-static solution under different parameter conditions. This choice successfully met the criteria of the 5 % energy fraction as other trials led to inconsistent results of the load-slip behaviour and the ratio of the kinetic to the internal energy of the system exceeded the limit of 10%.
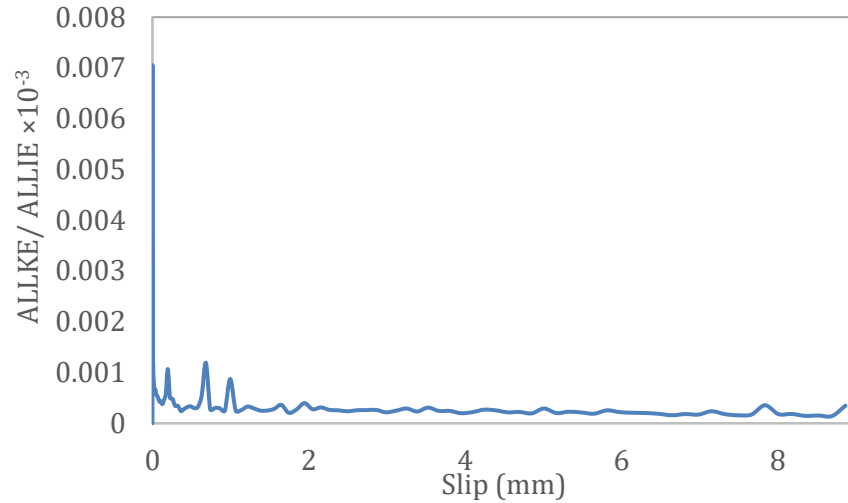
Fig. 35: Ratio of kinetic energy to internal energy versus slippage at 10 mass scaling

Eventually, the total load that is applied to the push-out test is computed by summing up all the reaction forces on the displacement surface which is the thickness of the flange. Also, the slippage is calculated by taking the average displacement on the displacement surface. Thereafter, the Load-slip curve is established using these values from the history field output by combining them together.

The initial loading cycles were not carried out in the FE modelling due to the observations made from the tests performed by Lam and El-Lobody (2005). They found that there is a few or no effects from the initial cycles. In addition, the load–slip behaviour was not affected by the initial cycles at all.

2.8   Thermal analysis model

According to Kruppa and Zhao (1995), assessing the fire behaviour of composite beams is divided into two parts as shown in Fig. 36.
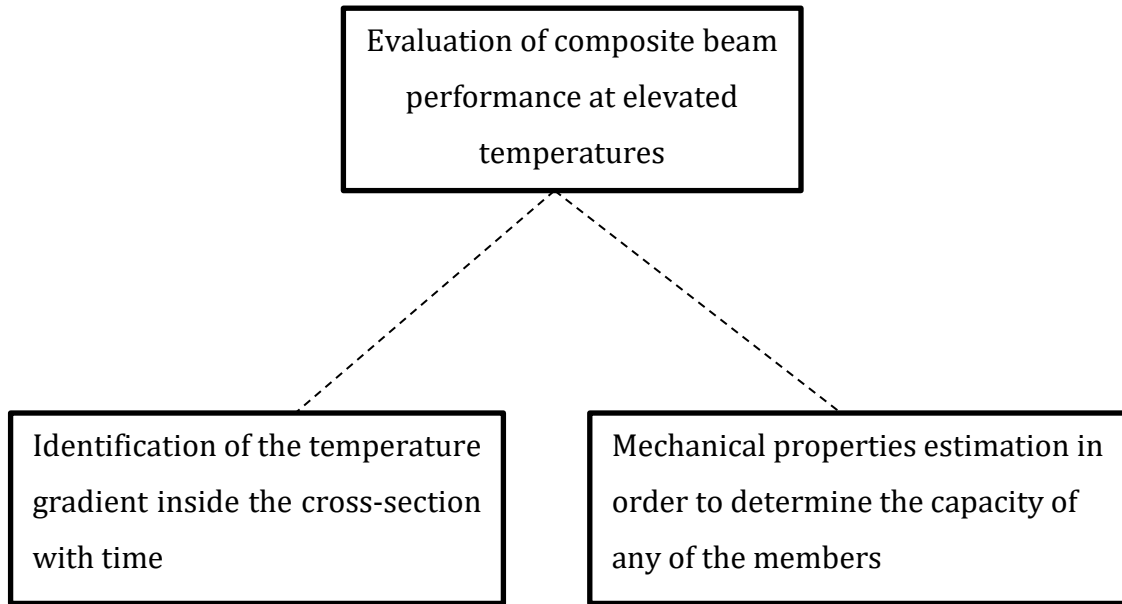
Fig. 36: overview of assessing the fire behaviour in composite beams (Kruppa and Zhao, 1995)

2.8.1 Temperature distribution in cross-section

Kruppa and Zhao (1995) developed a heat transfer analysis using TASEF-2 program for fire exposure of a protected and unprotected steel sections and by assigning heat flux as a boundary condition through the composite section. They observed that within the concrete slab, a significant thermal gradient is identified with a considerable difference between the exposed and unexposed side of the slab to fire. For the steel section, a significant difference in temperature between the upper and lower steel flanges with a web temperature nearly an average between the steel flange temperatures. Furthermore, the insulating effect of concrete slab resulted in a lower temperature in upper flange than the lower flange. In case of protection, Lower concrete temperature is noticed above the steel section.

The temperature gradient inside the solid slab was modelled in a simplified way such that a two-dimensional heat transfer problem was considered only and the longitudinal temperature distribution was assumed to be uniform. The temperature gradient has been adopted from the model of Kruppa and Zhao (1995) as indicated in Fig. 37
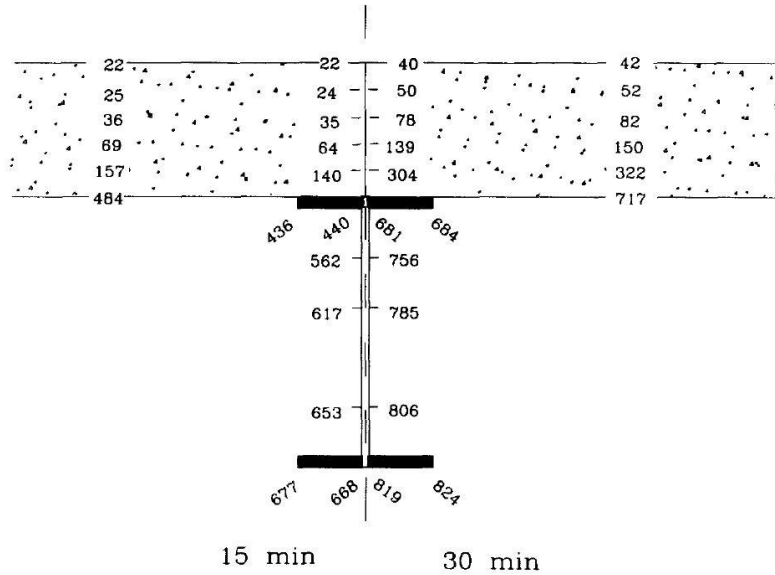
Fig. 37: Field of temperature in a composite beam with solid slab exposed to ISO 834
standard fire based on numerical analysis (Kruppa and Zhao, 1995)

Concrete slab, steel flange and headed shear stud sections were modelled with three-dimensional, 20-node quadratic heat transfer brick (DC3D20) With different thermal material properties. The thermal material properties of both concrete and steel were modelled according to the specifications of Eurocode 4 "En1994-2-2". These thermal material properties are temperature dependant and they include thermal conductivity, coefficient of thermal expansion and density. A heat transfer steady-state step was performed in ABAQUS such that the temperatures of the top and the bottom of the concrete block were specified as boundary conditions for the thermal analysis. This has been done using a ramp amplitude with a uniform distribution. Such approach successfully led to a thermal gradient inside the concrete slab with a curvilinear distribution of temperature across the depth. This approach is considered fairly enough for the sake of having a different temperature distribution for performing the thermo-mechanical analysis with main focus on applying the shear force on the headed stud at elevated temperatures.

2.8.2 Thermal material properties of concrete and steel at elevated temperatures

2.8.2.1 Concrete

According to Eurocode 4 "En1994-2-2", the thermal conductivity of normal weight concrete (λ_c) could be determined from the following equations which provide an upper limit and a lower limit:

$$\lambda_c \text{ upper limit } \left(\frac{W}{mk}\right) = 2 - 0.245\left(\frac{\theta_c}{100}\right) + 0.0107\left(\frac{\theta_c}{100}\right)^2 \qquad \text{Eq. (21)}$$

$$\lambda_c \text{ lower limit } \left(\frac{W}{mk}\right) = 1.36 - 0.136\left(\frac{\theta_c}{100}\right) + 0.057\left(\frac{\theta_c}{100}\right)^2 \qquad \text{Eq. (22)}$$

for 20 °C < θ_c < 1200 °C, where θ_c is the concrete temperature

The upper limit values are recommended by Eurocode 4 and they were used in the thermal analysis. The thermal conductivity values are illustrated in Table 12.

Table 12: Thermal conductivity of concrete at different temperatures calculated using Eq. (23)

θ (°C)	λ_c (W/mm.K)
20	1.95×10^{-3}
100	1.77×10^{-3}
200	1.55×10^{-3}
300	1.36×10^{-3}
400	1.19×10^{-3}
500	1.04×10^{-3}
600	9.20×10^{-4}
700	8.10×10^{-4}
800	7.20×10^{-4}

In order to calculate the thermal expansion of concrete, the thermal elongation ($\Delta L/L$) of concrete has to be defined first. The type of aggregate of the concrete is assumed to be calcareous. According to Eurocode 2, the thermal elongation ($\Delta L/L$) of concrete with calcareous aggregates can be calculated from Eq. (24). The coefficient of thermal expansion

was then derived from Eq. (25) which is the derivative of the thermal elongation equation with respect to temperature. The values of concrete coefficient of thermal expansion are presented in Table 13.

$$\Delta L/L = -1.2 \times 10^{-4} + 6 \times 10^{-6}\, T_c + 1.4 \times 10^{-11}\, T_c^{\,3} \quad 20\ °C < T_c < 805\ °C \qquad \text{Eq. (24)}$$

$$\alpha_c = 6 \times 10^{-6} + 4.2 \times 10^{-11}\, T_c^{\,2} \qquad\qquad 20\ °C < T_c < 805\ °C \qquad \text{Eq. (25)}$$

Table 13: Coefficient of thermal expansion of concrete at different temperatures calculated using Eq. (26)

θ (°C)	α_c (1/°C)
20	6.02×10^{-6}
100	6.42×10^{-6}
200	7.68×10^{-6}
300	9.78×10^{-6}
400	1.27×10^{-5}
500	1.65×10^{-5}
600	2.11×10^{-5}
700	2.66×10^{-5}
805	3.32×10^{-5}

According to the Eurocode 2 "EN 1992-1-2", Eq. (25) is proposed to calculate the concrete density at the elevated temperatures. The density of concrete at normal temperature was taken as 2.6455×10^{-9} ton/mm^3. The values of concrete density at elevated temperatures are presented in Table 14.

$$\rho(T) = \rho(20°C) \qquad\qquad\qquad\qquad 20\ °C < T_c < 115\ °C$$

$$\rho(T) = \rho(20°C)\left(1 - \frac{0.02(T-115)}{85}\right) \qquad 115\ °C < T_c < 200\ °C \qquad \text{Eq. (27)}$$

$$\rho(T) = \rho(20°C)\left(0.98 - \frac{0.03(T-200)}{200}\right) \qquad 200\ °C < T_c < 400\ °C$$

$$\rho(T) = \rho(20°C)\left(0.95 - \frac{0.07(T-400)}{800}\right) \qquad 400\ °C < T_c < 1200\ °C$$

Table 14: Density of concrete at different temperatures calculated using Eq. (28)

θ (°C)	ρ_c (ton/mm³)
20	2.65×10^{-9}
100	2.65×10^{-9}
200	2.65×10^{-9}
300	2.55×10^{-9}
400	2.51×10^{-9}
500	2.49×10^{-9}
600	2.47×10^{-9}
700	2.44×10^{-9}
800	2.42×10^{-9}

2.8.2.2   Steel

According to Eurocode 4 "En1994-2-2", the thermal conductivity of steel (λ_s) which is valid for structural and reinforcing steel could be determined from the following equations:

$$\lambda_s \left(\frac{W}{mk}\right) = 54 - 0.0333\ T_s \quad \text{for } 20\ °C < T_s < 800\ °C$$

Eq. (29)

$$\lambda_s \left(\frac{W}{mk}\right) = 27.3 \qquad \text{for } 800\ °C < T_s < 1200\ °C$$

Eq. (30)

Table 15: Thermal conductivity of steel at different temperatures calculated using Eq. (31)

θ (°C)	λ_s (W/mm.K)
20	0.053334
100	0.05067
200	0.04734
300	0.04401
400	0.04068
500	0.03735
600	0.03402
700	0.03069
800	0.02736

According to the Eurocode 4, the thermal elongation ($\Delta L/L$) of steel can be calculated from Eq. (28). The coefficient of thermal expansion of steel was then derived from Eq. (29) which is the derivative of the thermal elongation equation with respect to temperature. The values of steel coefficient of thermal expansion are presented in Table 16.

$$\Delta L/L = -2.416 \times 10^{-4} + 1.2 \times 10^{-5}\, T_s + 0.4 \times 10^{-8}\, T_s{}^3$$

$$20\,°C < T_s < 750\,°C \qquad\qquad \text{Eq. (32)}$$

$$\alpha_s = 1.2 \times 10^{-5} + 0.8 \times 10^{-8}\, T_s{}^2 \qquad 20\,°C < T_s < 750\,°C \qquad \text{Eq. (33)}$$

Table 16: Coefficient of thermal expansion of steel at different temperatures calculated using Eq. (34)

θ (°C)	α_s (1/°C)
20	1.22×10^{-5}
100	1.22×10^{-5}
200	1.22×10^{-5}
300	1.22×10^{-5}
400	1.22×10^{-5}
500	1.22×10^{-5}
600	1.22×10^{-5}
700	1.22×10^{-5}
750	1.8×10^{-5}

The density of steel was considered to be independent of the steel temperature. The value was taken as 7850 kg/m^3 as per recommendation from Eurocode 4.

2.8.3 Mechanical Material properties at elevated temperatures

2.8.3.1 Concrete

Eurocode 4 "En1994-2-2" proposed Eq. (30) for the stress-strain relationship for concrete at different elevated temperatures:

$$\sigma_{c,\theta} = f_{c,\theta}\left\{ 3\left(\frac{\varepsilon_{c,\theta}}{\varepsilon_{cu,\theta}}\right) / \left(2 + \left(\frac{\varepsilon_{c,\theta}}{\varepsilon_{cu,\theta}}\right)^3\right)\right\} \qquad \text{Eq. (35)}$$

$$f_{c,\theta} = k_{c,\theta}\, f_c \qquad \text{Eq. (36)}$$

Where, $f_{c,\theta}$ is concrete compressive strength at temperature θ (MPa); $k_{c,\theta}$ is concrete compressive strength reduction factor at temperature θ ; $\varepsilon_{c,\theta}$ is concrete strain at temperature θ ; $\varepsilon_{cu,\theta}$ is concrete strain at stress equal to $f_{c,\theta}$.

Normal weight concrete with calcareous aggregates was chosen in the analysis and the corresponding values for the $k_{c,\theta}$ and $\varepsilon_{cu,\theta}$ at different temperatures are presented in Table 17 as per Eurocode 4.

Table 17: Compressive stress-strain relationship parameters at different temperatures as per Eurocode 4.

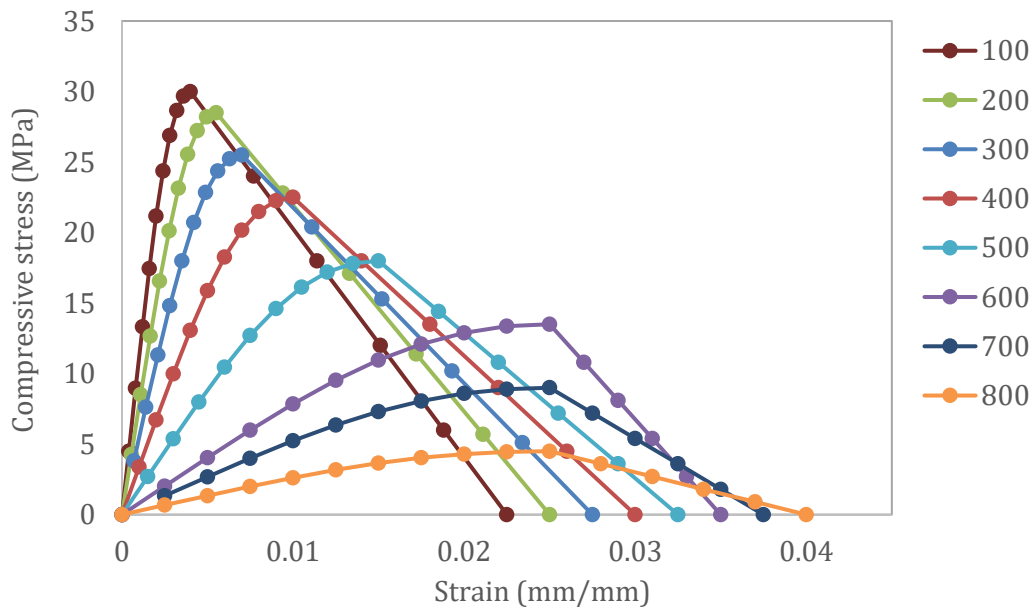| θ (°C)	$k_{c,\theta}$	$\varepsilon_{cu,\theta}$
20	1	0.0025
100	1	0.004
200	0.97	0.0055
300	0.91	0.007
400	0.85	0.01
500	0.74	0.015
600	0.6	0.025
700	0.43	0.025
800	0.27	0.025

Fig. 38: compressive stress-strain curve for concrete at elevated temperatures

2.8.3.2 Steel
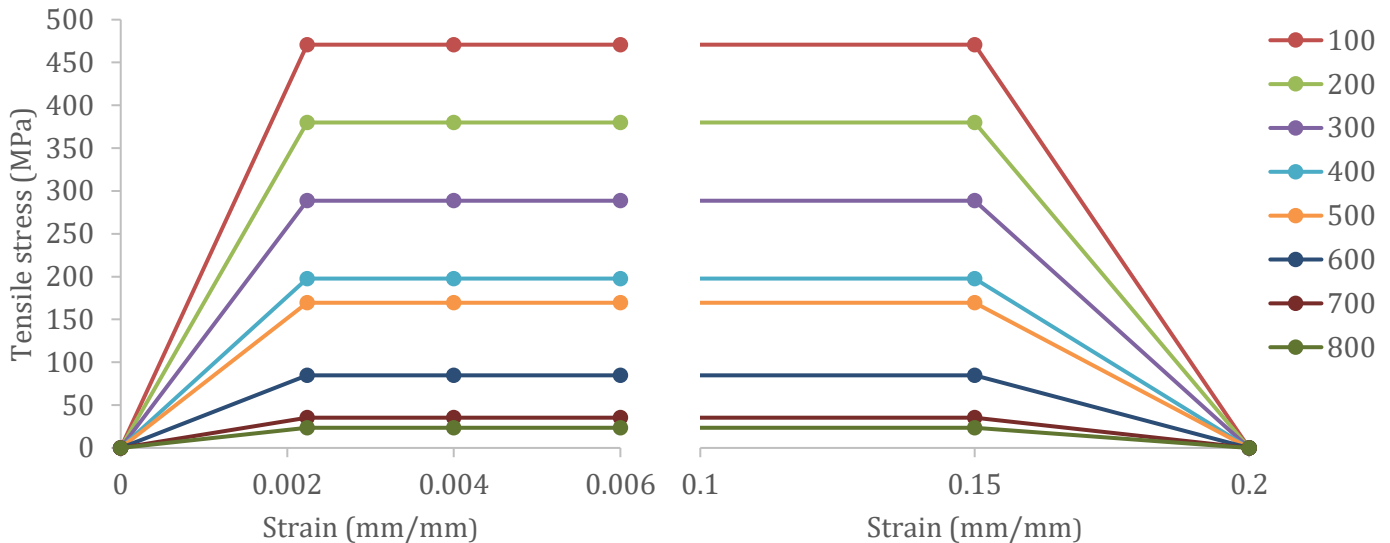
Fig. 39: Tensile stress-strain curve for steel at elevated temperatures

The thermal analysis and the mechanical model were conducted independently. The thermal analysis was conducted first to get the temperature distributions inside the slab. The thermal model was carried out with heat transfer elements. Then, the thermo-mechanical analysis was performed using structural elements and the nodal temperatures obtained in the thermal model were implemented as a predefined field.

Following that, the temperature-dependent material properties and the applied load were introduced. In order for the models to be compatible, the thermal model and structural model meshes have to be identical. This was ensured by using the option "compatible" while predefining the temperature from the thermal model into the thermo-mechanical one.

After inputting the yield stress and the in-elastic strain in ABAQUS for concrete and steel at different elevated temperatures, the analysis was carried out by interpolating the non-linear properties at different temperatures. Inserting these properties has to be done with care because if the values are not entered in a similar correct sequence at different temperatures, the program fails to interpolate the material properties since there is as temperature gradient within the slab.

3. Results and Discussion

3.1 Normal temperature

After observing and trying various strategies for performing the push-out test using the dynamic analysis, the Load-slip curves were established to assess the behaviour of the headed studs. The concrete material model comprising the compression and tension behaviour as well as the properties of the structural steel used play a significant role in the development of the load-slip curves. The push-out test on the solid slab was done using the concrete damaged plasticity model of 30 MPa concrete compressive strength and a perfect elastic-plastic steel of yield strength 470.8 MPa. Fig. 40 shows the resulted load-slip curve from the analysis. Since the analysis has been performed using the explicit solver, the analysis keeps running even after occurrence of failure and the load keeps increasing due to other numerical resistance from the undamaged concrete. The ultimate capacity of the connection is assumed in these analyses to occur as soon as the curve drops to 20 % of the maximum load reached and the slippage at failure is considered to be at this drop. In the context of this definition, the stud achieved a capacity of 100 kN along with a relative slippage around 9 mm. The numerical strength of the stud was compared with the design strengths equations for the concrete and the stud material from Eurocode 4. The dashed coloured lines in Fig. 40 indicate the predicted capacities of the studs. The predicted strength for the stud material from Eurocode 4 has a value of 106.7 kN and the capacity for concrete failure is 104 kN. It can be deduced that the numerical strength somewhat gave reasonable results compared to the predicted strengths according to the provisions of Eurocode 4. The predicted capacity for the composite slab was calculated with applying the reduction factor for composite slab with ribs parallel to the steel sheeting. It is obviously seen from Fig. 40 that the load-slip curves for both slabs behaved more or less in the same manner. Experiments by Chen et al. (2016) for composite slabs with parallel profiled sheeting achieved a capacity of the stud of 100 KN adding that the Eurocode 4 produced conservative estimates.
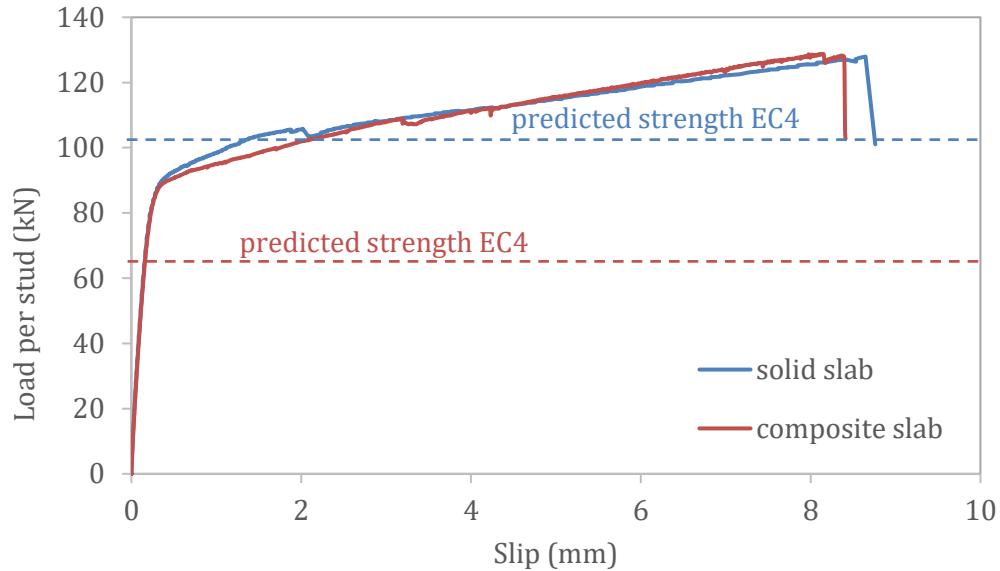
Fig. 40: Load-slip curve for 30 MPa concrete and 19 mm ×100 mm stud

3.1.1 Failure mechanism analysis at normal temperature

At ambient temperature, the connection experienced failure due to yielding of the stud at its base. This phenomenon occurred first as the stresses was gradually increasing from the base and rising along the height of the stud until almost 2/3 of the stud from its base reached the yielding stress as shown in Fig. 41. The reason for yielding of the stud above 10 mm from its base because the stud was fully embedded in the concrete but yielding was supposed to occur at the base only. The analysis predicted that the stud yielded before concrete crushing occurred. Just after yielding of the stud at its base, the concrete elements surrounding the shear stud hit their full compressive stress. This behaviour was predicted to occur at ambient temperature as per the conclusions of other researchers that was previously discussed. Fig. 42 demonstrates the predicted failure mode with the relative slippage that occurred between the concrete and steel section. It can be observed that the maximum compressive stresses in the concrete occurred at the lower half of the stud with a distribution like a bell-shaped curve along the cross section of the specimen. The same failure mode was observed in the composite slab but it was accompanied by separation of the corrugated sheet from the concrete block as shown in Fig. 43. This separation is supposed to occur in the experimental push-out test with damage in the sheet in the area around the stud after its fracture.
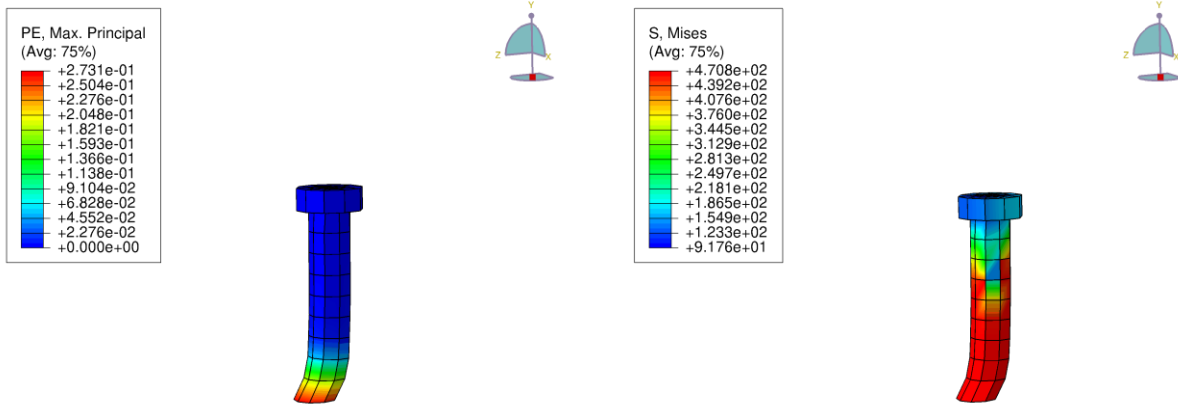
Fig. 41: plastic strain components (PE) contours and stress distribution of the shear stud after failure
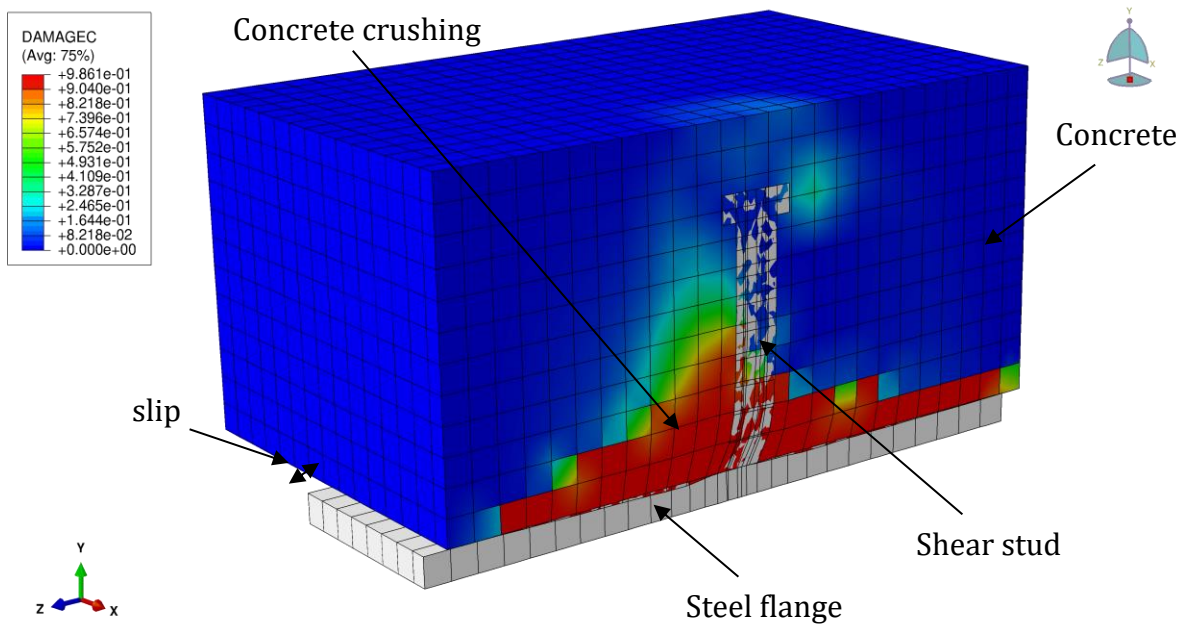

Fig. 42: cut view showing the failure mode of solid slab and the occurred slippage
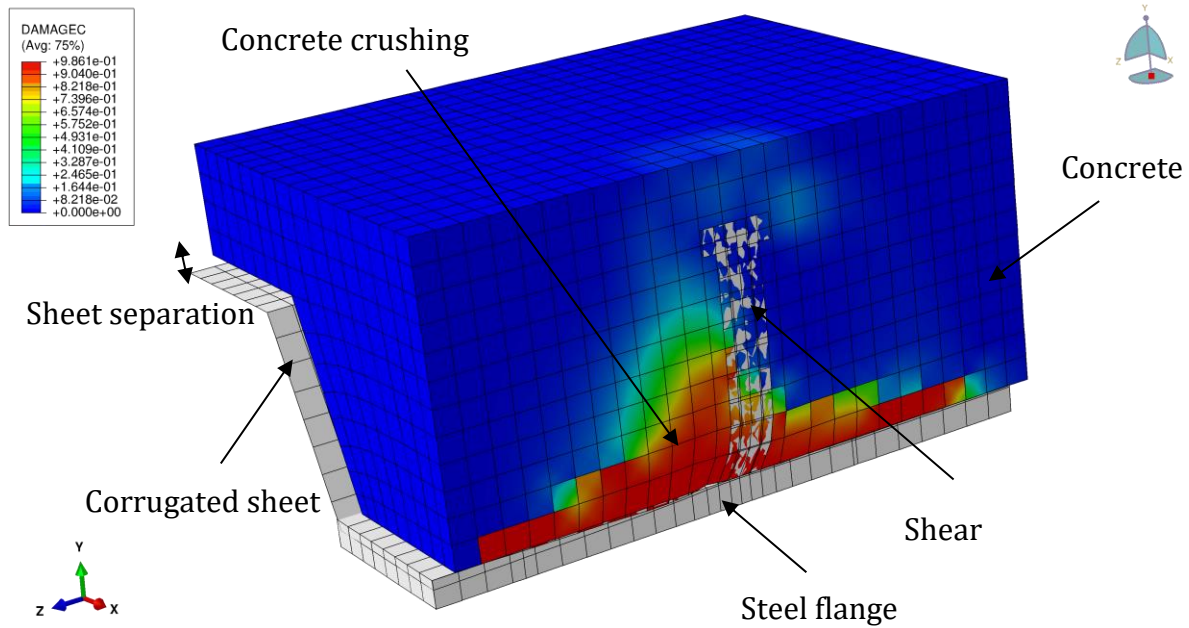
Fig. 43: cut view showing the failure mode of composite slab accompanied by sheet separation from concrete

3.2 Thermal analysis for solid slab

The steady-state heat transfer analysis was conducted twice. The first was carried out at 15 minutes and the other at 30 minutes adopting a temperature boundary condition from the numerical model developed by Kruppa and Zhao (1995). A temperature gradient can be observed in both the concrete slab and the shear stud as shown in Fig. 44 and Fig. 45. The temperature reached at the bottom of the stud was exactly the same as the flange for both models. At 10 mm from the bottom of the stud, the temperature reached around 450 °C and 650 °C at 15 and 30 minutes respectively. The temperature at the head reached about 190 °C at 15 minutes and around 275 °C at 30 minutes. The most important temperatures in the push-out test are those reached at the bottom of the stud and at around 10 mm from the base of stud where the shear force is supposed to develop. However, the temperatures at the head may be of importance in the large-scale tests where the whole composite beam with the slab is tested under bending and the stud head is expected to resist a tension force. The

temperature distribution along the stud height and the concrete depth are illustrated in Fig. 46 and Fig. 47.

15 minutes
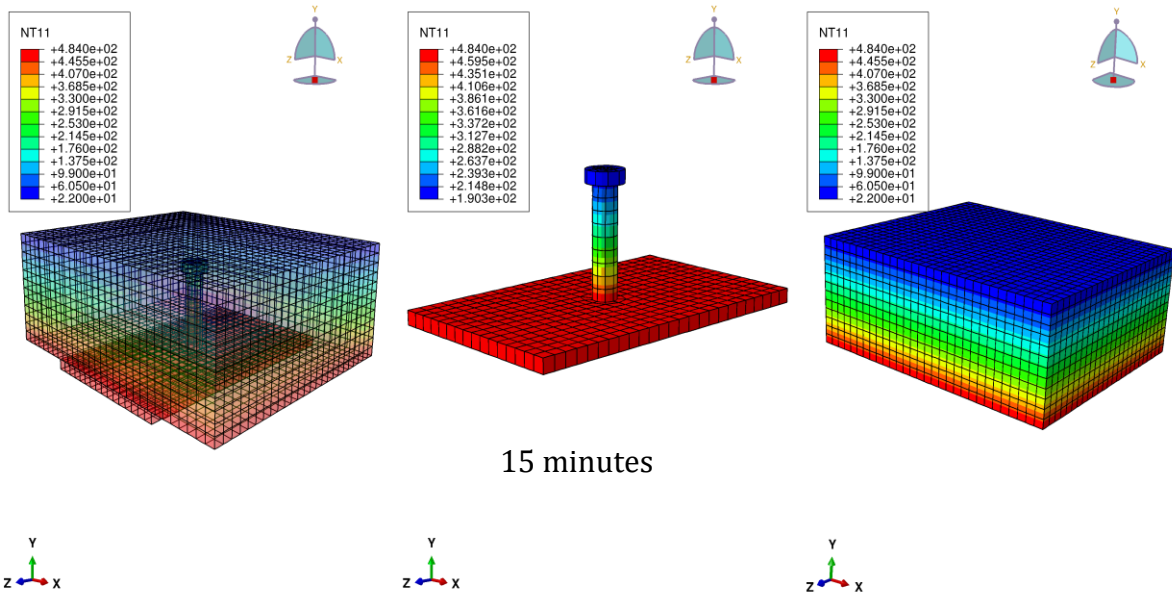
Fig. 44: Temperature distribution in the headed stud and the solid concrete slab at 15 minutes
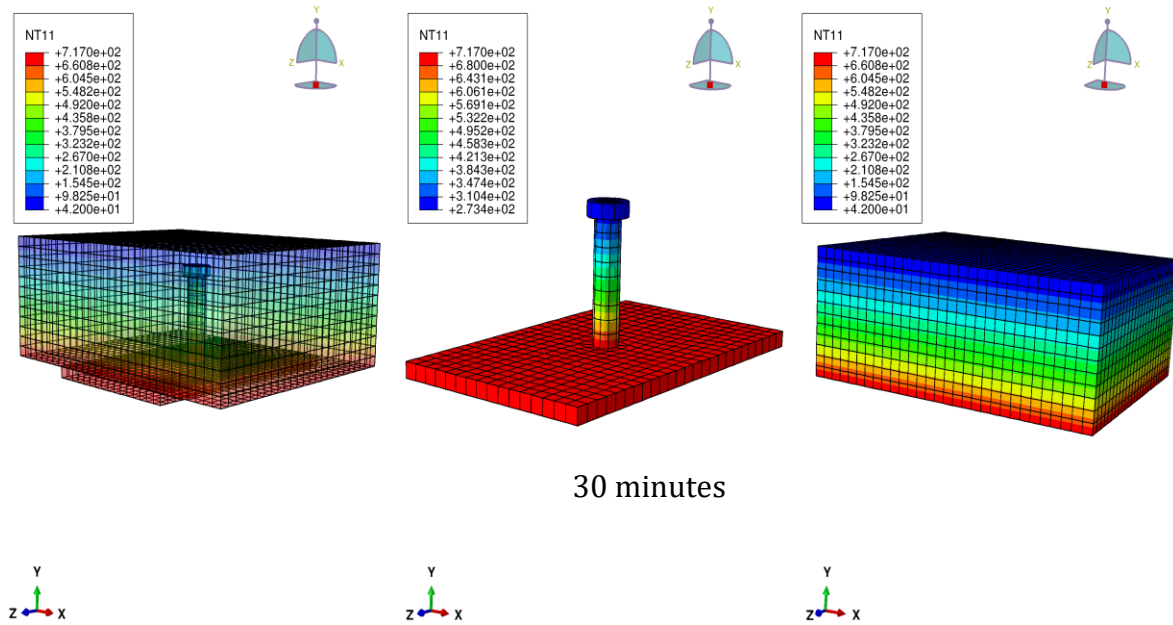

30 minutes

Fig. 45: Temperature distribution in the headed stud and the solid concrete slab at 30 minutes
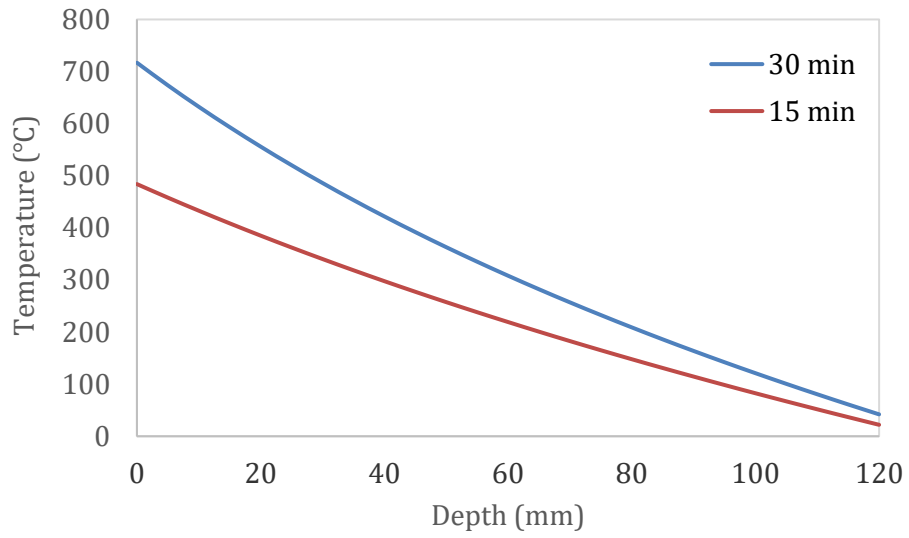
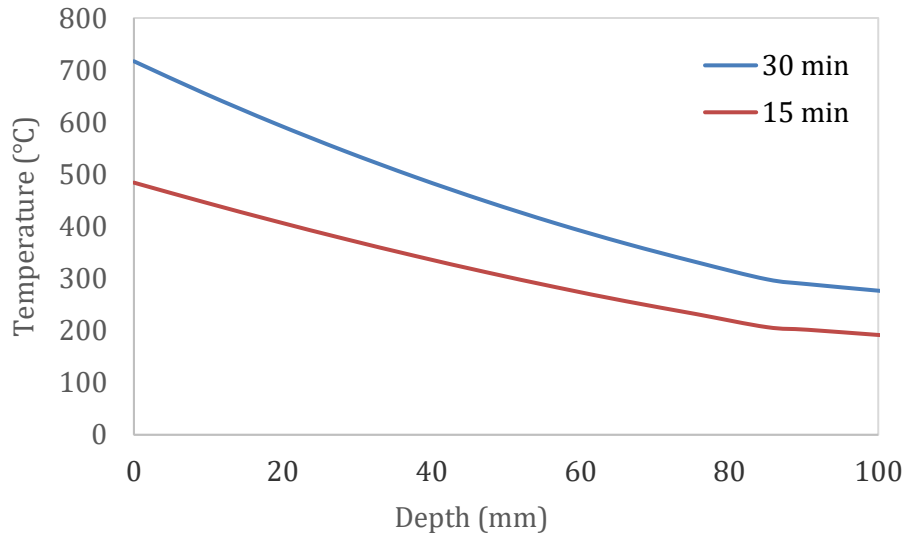Fig. 46: Isotherms in the solid concrete slab along the depth

Fig. 47: Typical temperature distribution along the axis of the shear stud

3.3 Thermo-mechanical analysis of the solid slab

As discussed in section 2.8.3, the rise in temperatures of both steel and concrete resulted in a reduction of their mechanical properties. Additionally, the difference in the thermal expansion between the concrete and the steel contributed to the increase of the Shear force on the shear stud. The temperature gradient in the slab is considered essential to be studied due to its effect on the floor performance and the stresses on the shear stud. From the graph of the reduction of steel strength at elevated temperatures in Fig. 39, it is obvious that the steel strength reduced significantly above 500 °C and reached just above 35 % of its strength at ambient temperature. This will always lead to a dominant failure of the connection due to shearing off of the studs. Fig. 48 shows the change in the load-slip behaviour of the studs at elevated temperatures. A total reduction in the capacity of the stud was witnessed compared to its capacity at ambient temperature. The stud strength nearly reached 64 % and 25 % of its ambient strength after 15 minutes and 30 minutes respectively. Regarding the slippage, it dropped down from 9 mm at normal temperature to just above 4.5 mm at 15 minutes and slightly before 4 mm at 30 minutes.

The numerical strength of the stud at elevated temperature was compared with the design strengths equations for the concrete and the stud material from Eurocode 4 with their reduction factors. The two reduction factors mentioned in Eurocode 4 for the stud and concrete at elevated temperature θ °C are not clear enough for the location where the temperature should be taken for both the stud and the concrete since there is a temperature gradient in whole slab.

The bottom of the shear stud temperature has been chosen by some researchers as a reference temperature, and the shear stud strength reduction is identified based on this reference temperature (Dara, 2015). Never the less, it is recommended by Eurocode 4 to take the values of these two temperatures as a percentage from the temperature of the upper flange of the beam such that the temperature of the shear stud may be taken 80% and the temperature of concrete 40% of the upper flange. In order to compare the results with the Eurocode 4 predictions, the approach of taking the steel and concrete temperatures as percentages from the upper flange temperature was adopted for the Eurocode 4 equations.

This has resulted in a predicted capacity of stud steel of 38 kN and concrete shear failure of 99 kN at 15 minutes. Also, a predicted capacity of stud steel of 23 kN and concrete shear failure of 90 kN at 30 minutes.
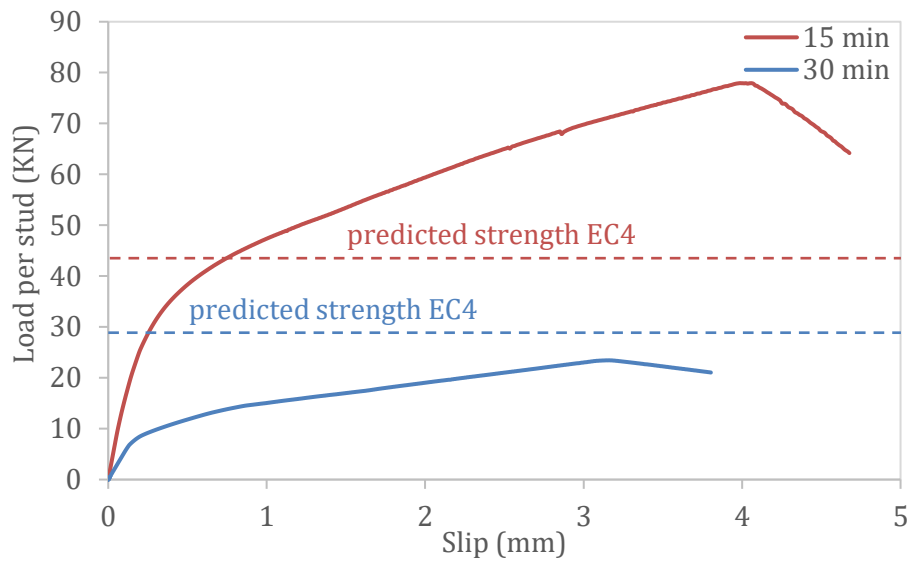
Fig. 48: Load-slip curve for the thermo-mechanical analysis of the solid slab at 15 and 30 minutes

The damage parameters were not accounted for in the CDP model at elevated temperatures. Instead, the corresponding plastic strain components (PE) contours were used to demonstrate the reached plasticity of the push-out test model as shown in Fig. 49 and Fig. 50

3.4   Validation of the model

In order to validate accuracy of the finite element model, the push-out tests conducted by Lam and El lobody (2005), Chen et al. (2016) and Mirza and Uy (2009) were compared with the numerical model presented in this thesis at normal and elevated temperatures. It is worth mentioning that the numerical push-out tests conducted by different researchers were with different material models and properties. However, the existing results were presented for a rough comparison between the different load-slip curves since no experimental work was done to validate the numerical model.

Fig. 49: cut view showing the plastic strain components (PE) contours at 15 and 30 minutes
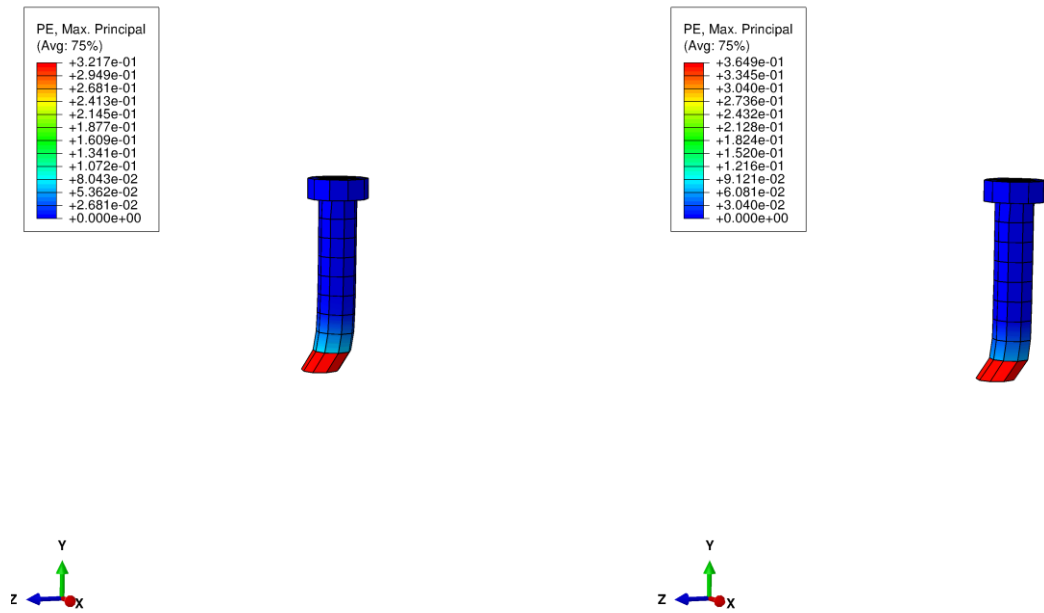
Fig. 50: plastic strain components (PE) contours for the stud at 15 and 30 minutes

At normal temperature, it is observed that the load-slip curve of the FE model for solid slab witnessed a different ductility than that of the model by Lam and El lobody (2005). It should be taken into account that the model by Lam was not performed with the CDP model but with the option "Plastic" in ABAQUS which treat the concrete with the same behaviour at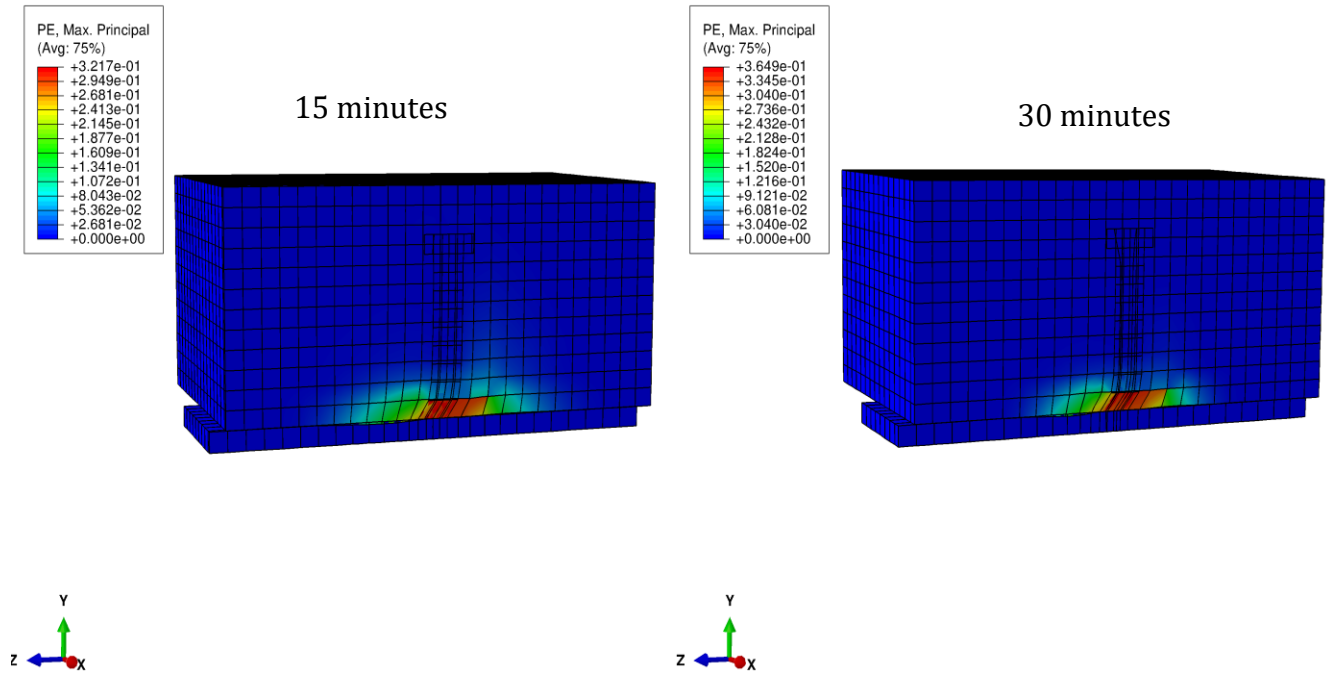 compression and tension. For the composite slab, a comparable value of slippage for the FE model was noticed with the model by Chen et al. (2016) but again with a different ductility of the load-slip curve. The load-slip curve by Chen et al. (2016) experienced the same trend as the one by Lam and El lobody (2005) but with a higher value of slippage.

At elevated temperatures, the FE model at 15 and 30 minutes was compared with the model performed by Mirza and Uy (2009) at 30 minutes. The FE results revealed a degree of somewhat close agreement especially in the occurred slippage and the slope of the elastic part of the load-slip curve. However, a deviation in the ultimate load reached was observed. The reason for this is the difference in the temperature distribution for the thermal analysis of both models as the model by Mirza was adopted from Lamont et al. (2004) while the conducted FE model was adopted from Kruppa and Zhao (1995).
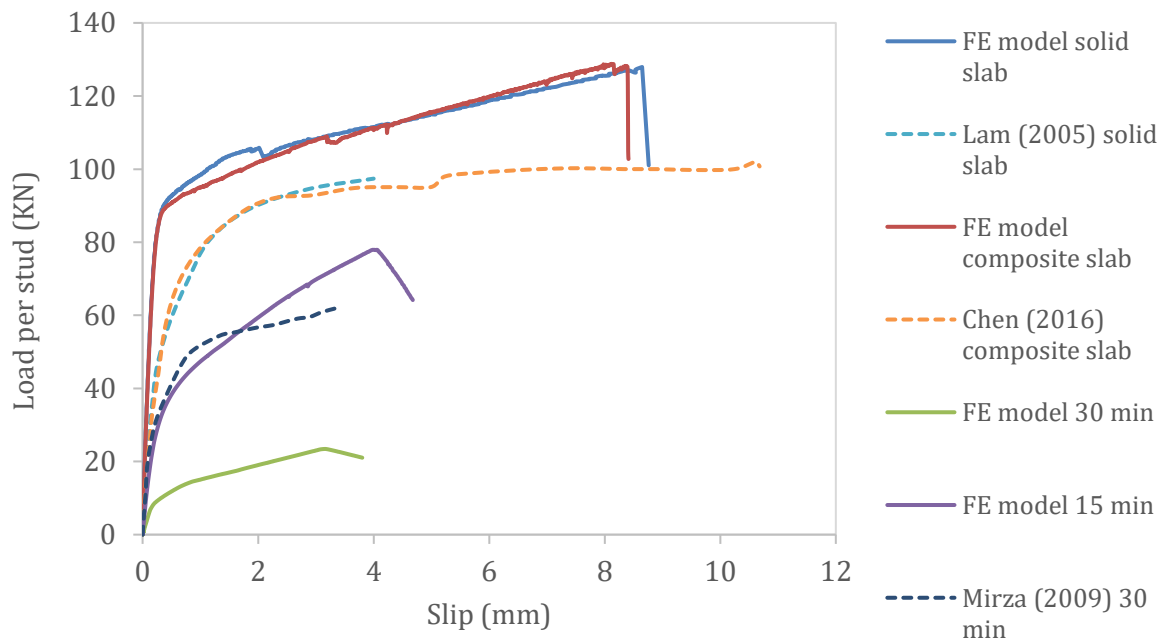
Fig. 51: Comparison between the FE model and existing results

3.5   Convergence study

A convergence study was carried out on the push-out test model to evaluate the sensitivity of different mesh sizes on the numerical results. The accuracy of the results is likely to be influenced by the mesh element size. As per mentioned earlier in section 2.2 that the whole model with its different components was meshed with the same mesh size in order to ensure a reliable contact between them. Three different sizes of element were investigated, a coarse mesh of 20 mm × 20 mm, a medium-sized mesh 15 mm × 50 mm and a fine mesh of 10 mm × 10 mm as shown in Fig. 52. The different simulations done with different element sizes were conducted with a loading rate with velocity of 0.5 mm/s and a mass scaling of 10 which proved to give consistent results for the quasi-static solution. The numerical results of the different mesh sizes were evaluated and the optimum size which gave reasonable results in an efficient computational time was further considered in the rest of the FE models developed.

10 mm × 10 mm   15 mm ×15 mm   20 mm × 20 mm
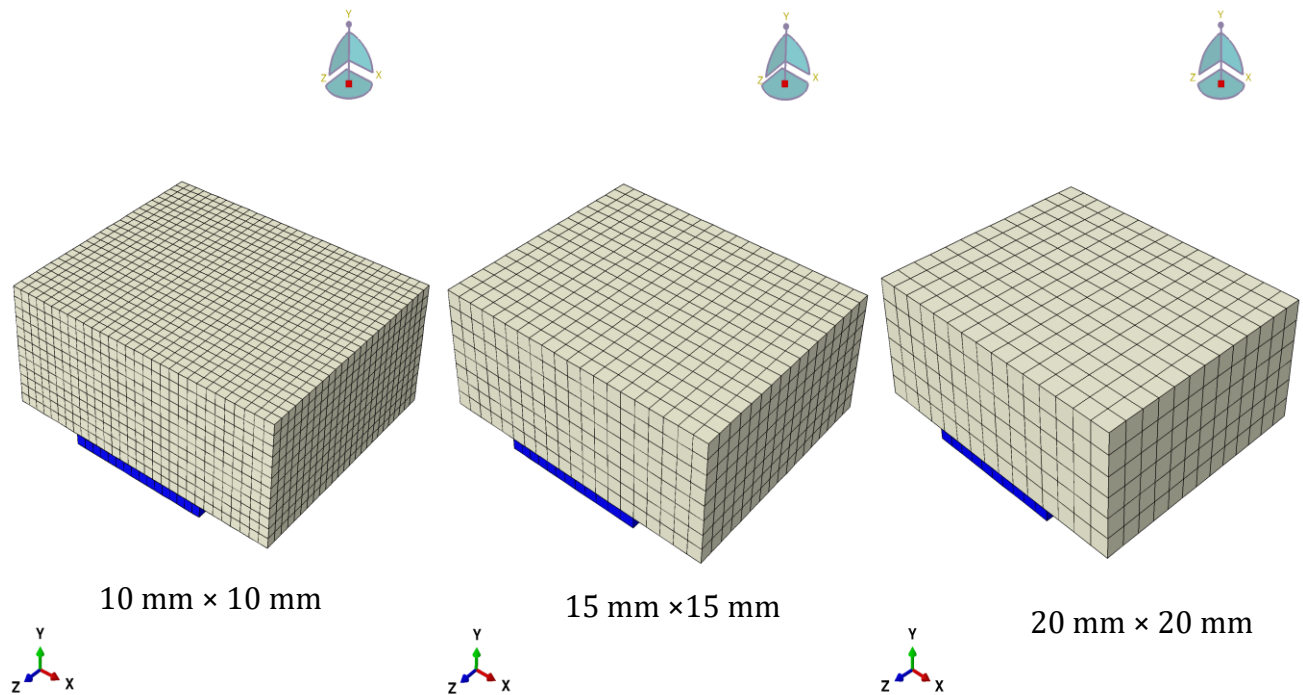
Fig. 52: Different mesh element sizes
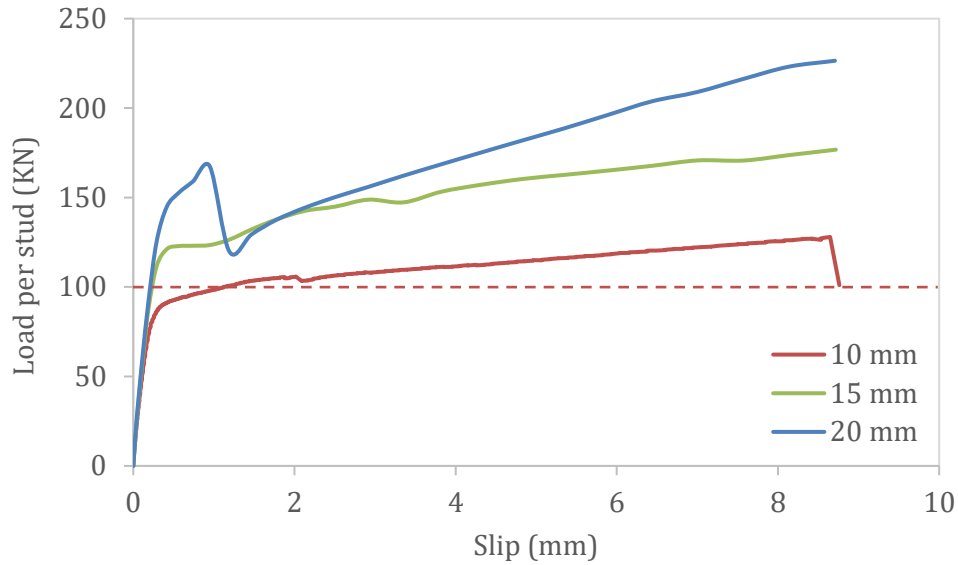
Fig. 53: Comparison of load-slip curves with different mesh sizes

It can be clearly seen from Fig. 53 that the coarse mesh of 20 mm × 20 mm extremely over-predicted the load-slip behaviour of the headed shear studs compared with the proposed capacity according to Eurocode 4. On the other hand, the fine mesh of 10 mm × 10 mm contributed to a comparable behaviour of the stud in the push-out test. The 10 mm × 10 mm mesh size was the most precise curve for the estimated capacity of the stud. With regards to the medium mesh size of 15 mm ×15 mm, it also over-predicted the strength and the load-slip behaviour of the stud with a continuous rate of increase. Accordingly, the 10 mm × 10 mm fine mesh is somewhat efficient to use due to its precision that was shown in the load-slip behaviour.

3.6   Parametric Study

A parametric study was conducted using three different dimensions of the stud 16 mm × 75 mm, 19 mm × 100 mm and 22 mm × 100 mm. This study was carried out to investigate the change in the load-slip behaviour with different dimensions of the headed studs. The cross-sectional area of a headed stud is well known to play a significant role in the shear connector resistance of composite beams. The same concrete strength of 30 MPa and a steel yield strength of 470.8 N/mm² were used. The numerical results were compared with the calculated values of shear strength equations in Eurocode 4. The dashed coloured lines in

Fig. 54 indicate the predicted capacities of the studs from Eurocode 4. It can be obviously seen from the results in Fig. 54 that the three-different dimensions experienced the same stiffness in the elastic region of the load-slip curve. The 22 mm × 100 mm headed stud accounted for the highest stud strength due to its large diameter, on the contrary, the 16 mm × 75 mm recorded the least strength which is reasonable. Regarding the relative slip, the highest slippage occurred for the 19 mm × 100 mm headed stud while the 16 mm × 75 mm and 22 × 100 mm studs had reached nearly the same slippage. The 16 mm × 75 mm stud achieved a capacity of 80 kN with a relative slippage of approximately 6 mm and the predicted capacity from Eurocode 4 has a value of 75 kN which agreed well with the numerical strength. For the 22 mm × 100 mm stud, the capacity recorded is 120 kN with a slippage just above 6 mm. The numerical slippage for the 22 mm × 100 mm stud is doubtful since it should be greater than that of both the 19 mm × 100 mm and the 16 mm × 75 mm studs.
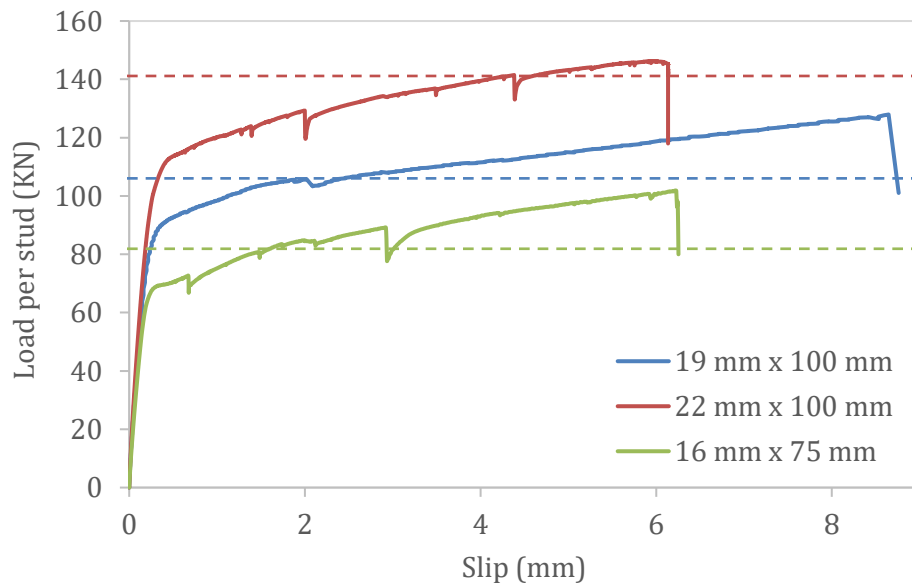
Fig. 54: Load-slip curves for various dimensions of headed studs in 30 N/mm² concrete

A parametric study was performed using different values of the dilation angle in the CDP model to investigate the sensitivity of these parameter on the load-slip behaviour of the stud. The same concrete strength of 30 MPa and a steel yield strength of 470.8 N/mm² were used with a 19 mm ×100 mm shear stud for the solid slab. As seen in

Fig. 55, the load-slip curve exhibits a major sensitivity to the dilation angle value. Increasing the value of the dilation angle from 15 to 45 demonstrated a significant increase in shear stud strength but with the same ductility.
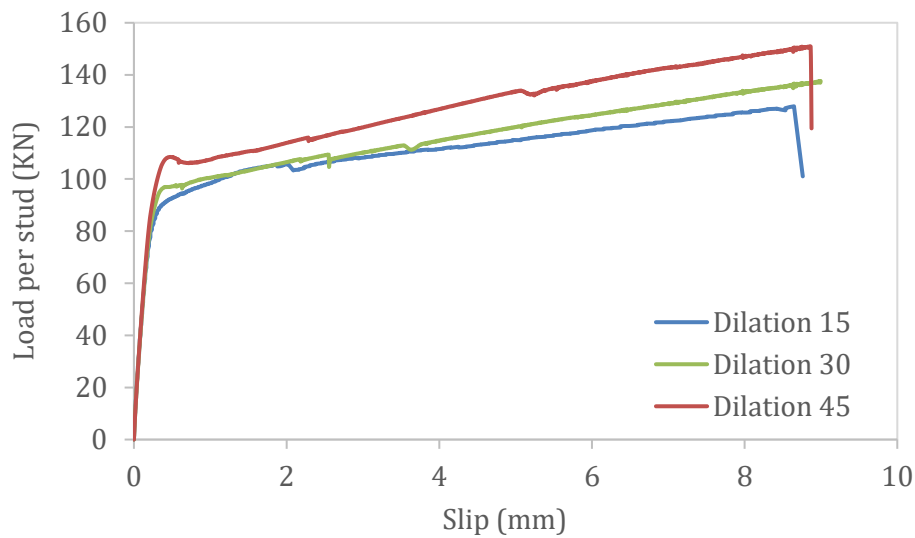
Fig. 55: Load-slip curves for various values of dilation angles in the CDP model in 30 N/mm² concrete

Furthermore, a parametric study was conducted to study the effect of the width of the slab on the capacity of the stud. It can be observed that all the push tests with different concrete block geometries behaved in more or less similar manner. An increase of 100 mm in the block from 300 mm to 400 mm width did not substantially change the behaviour of the load slip curve as illustrated in Fig. 57.

Moreover, for the trapezoidal section, the numerical model did not capture reduction in the load-slip behaviour since the failure mode is expected to be dominated by concrete crushing and cracking. As the stud is restricted by only the limited available area encountering the two slopes to avoid concrete crushing. This is explicitly demonstrated by

the reduction factor that should be applied to the stud strength in case of using a composite slab with ribs oriented parallel to the steel beam.

300 mm ×120 mm   400 mm×120 mm   Trapezoidal section
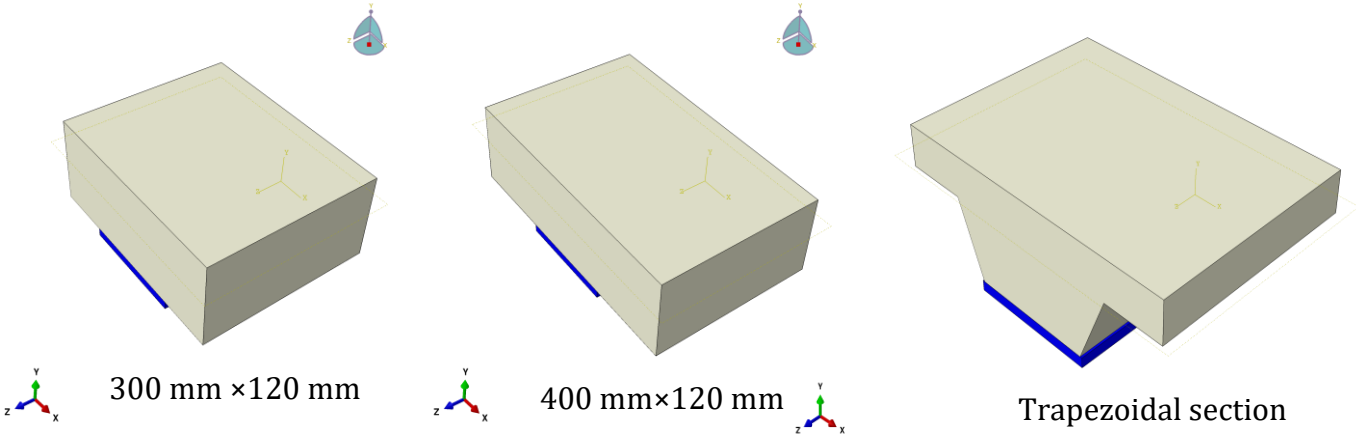
Fig. 56: Different concrete block geometries
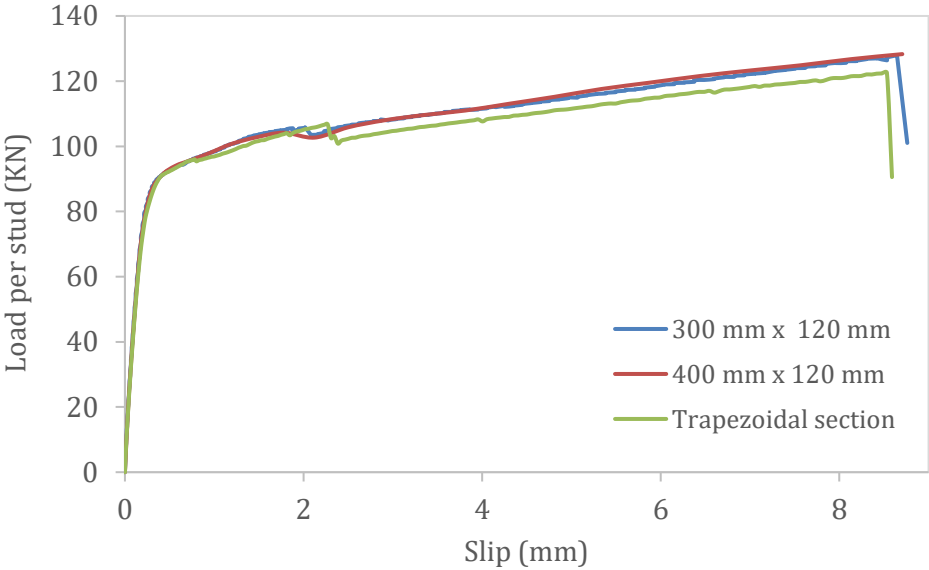
Fig. 57: Load-slip curves for various concrete block geometries

3.7 Uncertainties

There are numerous sources of uncertainty present in the FE model that may directly influence the results. One of these include the material properties used for modelling concrete at normal temperature. Many sources are available in literature to describe the concrete behaviour in tension and compression. Some values were assumed especially for the softening behaviour of concrete in compression. Furthermore, the uncertainty in the representation of the tension softening model of concrete using linear, bilinear or exponential function. Also, the values used for the plasticity parameters in the concrete damaged plasticity model proved to give different results especially for the dilation angle used as previously shown in the parametric study. Regarding the concrete at elevated temperatures, there was no information on how the values of plasticity parameters vary with temperature so the same values were assumed as in normal temperature. Another assumption was made in the concrete tensile model which is maintaining the same concrete tensile behaviour at elevated temperatures as in the normal temperature which is believed to decrease and affect the results.

From the modelling technique perspective, some uncertainties arise in the weld collar representation at the base of the stud with the steel flange. This has been done by merging the stud bottom with the steel flange. However, some researchers used another technique which is by increasing the diameter of stud at the base to simulate the weld. Another modelling perspective comprise the interaction of the stud with concrete. In the developed FE model, the stud was fully embedded in the concrete using the embedded constraints. Some researchers used the surface-to-surface contact to define the stud-concrete interaction using the normal and tangential behaviour without embedding the stud into the concrete. Nevertheless, it is argued by Katwal et al. (2018) that the relative movement between the stud and concrete is prevented and the actual slip behaviour of the stud will not be revealed in case the stud is fully embedded in the concrete. Some researchers (i.e. Lam and El lobody (2005)) only inserted a portion of the stud in the concrete to overcome this limitation.

Mesh refinement also plays an important role in the numerical results. Better predictions could have been made with mesh refining of the stud and in particular the region around the

stud bottom and the concrete where most of the stress concentration is actually present. The rate of the load applied is also a major issue in the Quasi-static analysis which affects the results obtained even though the kinetic and internal energy fraction of the system remain under the 5 % tolerance. This has been observed by running many simulations to investigate this issue

4. Summary and Conclusions

The numerical stud capacity turned out to be more dominated by the steel stud failure than the concrete cone failure. This is due to the complexity of modelling the concrete to act like the physical one in push-out tests despite the availability of the different models. Similar issues arise when modelling concrete at elevated temperatures as it is difficult to accurately define the compressive and tensile behaviour in ABAQUS. An alternative approach could be taken which is dealing with concrete to have the same behaviour at compression and tension. This approach resulted in an extreme deviation from the predicted load-slip behaviour. After observing different techniques, concrete damaged plasticity model was used to model concrete at elevated temperatures assuming the same tensile behaviour as in normal temperature. Also, at elevated temperatures, the ultimate load reached appeared to be dominated by the steel strength and not the concrete. In addition, by observing the plastic strains along the shear stud, the maximum principal plastic strains revealed occurrence of plasticity concentration at the bottom of the shear stud.

The explicit solver is mesh dependent and very sensitive to the loading rate applied. Small changes in the applied velocity and mass scaling could entirely change the load-slip behaviour and the results. In every trial attempted, the energy within the system was checked to avoid any inertia effects that could affect the results. The discrepancy in the results could be due to the way the ultimate load was defined unlike the static analysis where equilibrium takes place and the ultimate load could be defined easily. In the developed model, the plasticity parameters of the concrete damaged plasticity model were assumed to be temperature independent. Nevertheless, the parameters should vary with temperature. Additional work is needed to enhance the model in order to accurately predict the ultimate strength of the stud and the slippage at failure. Accurate results may be achieved if the nodes of the stud are tied to the nodes of the slab at the interface. The load-slip behaviour at elevated temperatures witnessed a reduction in the ultimate load reached. Not only the ultimate load reached but also the ductility in the load-slip curve itself and the relative slippage between the concrete and the steel section. The partial factor γ_v in the design resistance of headed stud connectors in solid slab at normal temperature in Eurocode 4

appeared to be too conservative as a value of 1.25 is recommended which decreased the predicted strength by 20 %. Likewise, the reduction factor for the composite slab with ribs parallel to the supporting beam is underestimating the stud capacity by 60 % which is too conservative.

4.1 Suggested future work

This thesis can be extended to further investigate the load-slip behaviour of solid and composite slabs as the current study was limited to a mesh size of 10 mm × 10 mm with a simplified way in the thermal analysis. The following recommendations are encouraged for future work:

1- A detailed transient heat transfer analysis could be conducted at 30, 60 and 90 minutes according to the ISO 834 to study the behaviour of the studs at different heating conditions.

2- The steady-state thermal analysis in this thesis has done only on the solid slab. It is necessary to perform a thermal analysis on the composite slab with the steel metal sheeting to capture any difference in behaviour of the headed studs compared to the solid slab.

3- The FE model was performed without inclusion of the reinforcing bars and it is suggested to take them into account to investigate the difference in behaviour of the load-slip curves.

4-Performing a full-scale test with a composite beam where the slab and the beam will be subjected to bending unlike the push-out test in which the stud only resists a pure shear force.

5- There is limited research and a gap in the performance of the headed studs when they are cooled down after experiencing severe fire conditions. An experimental work is suggested by exposing the studs to elevated temperatures and then testing them after being cooled down. This is numerically challenging as it would be difficult to find the reduction in the mechanical properties of concrete and steel after being cooled down.

6-The parametric study should be extended to cover various trapezoidal concrete block dimensions. Also, using double studs per row in the steel flange and different slab thickness.

References

ABAQUS Documentation (2016) ABAQUS User's Manual. Version 6.14, Hibbitt, Karlsson and Sorenson, USA.

Ali Shariati (2012) 'Various types of shear connectors in composite structures: A review', *International Journal of the Physical Sciences*, 7(22). doi: 10.5897/ijpsx11.004.

Bailey, C. G. (2004) 'Membrane action of slab/beam composite floor systems in fire', *Engineering Structures*, 26(12), pp. 1691–1703. doi: 10.1016/j.engstruct.2004.06.006.

Birtel, V. and Mark, P. (2006) 'Parameterised Finite Element Modelling of RC Beam Shear Failure', *Ababqus User's Conference*, pp. 95–108.

Carreira and Chu (1985) 'Relationship for Plain Concrete in Comprcssion Strcss € train', *ACI Structural Journal*, (November-December), pp. 797–804.

Chapman, J.C. and Balakrishnan, S., Experiments on Composite Beams, The Structural Engineer, 42, (11), November 1964.

Dara, S. (2015) 'Behavior of the Shear Studs in Composite Beams at Elevated Temperatures'. Doctor of Philosophy, The University of Texas at Austin

EN 1993-1-1 (2005): Eurocode 3: Design of steel structures - Part 1-1: General rules and rules for buildings [Authority: The European Union Per Regulation 305/2011, Directive 98/34/EC, Directive 2004/18/EC]

EN 1992-1-2 (2004): Eurocode 2: Design of Concrete Structures: Part 1-2: General Rules - Structural Fire Design.

E. Thorenfeldt, A. Tomaszewicz, and J. J. Jensen, "Mechanical properties of high-strength concrete and application in design," in Proc. Symposium on Utilization of High-Strength Concrete, Tapir, Trondheim, Norway, 1987, pp. 149-159.

Flint, G. *et al.* (2013) 'Recent Lessons Learned in Structural Fire Engineering for Composite Steel Structures', *Fire Technology*, 49(3), pp. 767–792. doi: 10.1007/s10694-012-0291-8.

Hillerborg, A, Modéer, M & Petersson, P-E, 1976. Analysis of crack formation and crack growth in concrete by means of fracture mechanics and finite elements. Cement and concrete research, 6(6), pp.773–781.

Imagawa, Y., Ohyama, O. and Kurita, A. (2012) 'Mechanical properties of shear stud during and after fire', *Structural Engineering International: Journal of the International Association for Bridge and Structural Engineering (IABSE)*, 22(4), pp. 487–492. doi: 10.2749/101686612X13363929517532.

J W Rackham (2014) *Composite Slabs and Beams using Steel Decking: Best Practice for Design and Construction*.

Jiang, S. C. *et al.* (2017) 'Behaviour and design of composite beams with composite slabs at elevated temperatures', *Advances in Structural Engineering*, 20(10), pp. 1451–1465. doi: 10.1177/1369433216682507.

Katwal, U., Tao, Z. and Hassan, M. K. (2018) 'Finite element modelling of steel-concrete composite beams with profiled steel sheeting', *Journal of Constructional Steel Research*, 146, pp. 1–15. doi: 10.1016/j.jcsr.2018.03.011.

Kruppa, J. and Zhao, B. (1995) 'Fire resistance of composite beams to Eurocode 4 Part 1.2', *Journal of Constructional Steel Research*, 33(1–2), pp. 51–69. doi: 10.1016/0143-974X(94)00014-9.

Lam, D. and El-Lobody, E. (2005) 'Behavior of Headed Stud Shear Connectors in Composite Beam', *Journal of Structural Engineering*, 131(1), pp. 96–107. doi: 10.1061/(asce)0733-9445(2005)131:1(96).

Lamont, S., Usmani, A. S. and Gillie, M. (2004) 'Behaviour of a small composite steel frame structure in a "long-cool" and a "short-hot" fire', *Fire Safety Journal*, 39(5), pp. 327–357. doi: 10.1016/j.firesaf.2004.01.002.

Ling-Zhu Chen , Guo-Qiang Li, S.-C. J. (2015) 'Experimental studies on the beahviour of headed stud shear connectors at elevated temepratures', *Acta Universitatis Agriculturae et Silviculturae Mendelianae Brunensis*, 53(9), pp. 1689–1699. Available at:

http://publications.lib.chalmers.se/records/fulltext/245180/245180.pdf%0Ahttps://hdl.handle.net/20.500.12380/245180%0Ahttp://dx.doi.org/10.1016/j.jsames.2011.03.003%0Ahttps://doi.org/10.1016/j.gr.2017.08.001%0Ahttp://dx.doi.org/10.1016/j.precamres.2014.12.

McAllister, T. P. *et al.* (2013) 'Structural Response of World Trade Center Buildings 1, 2 and 7 to Impact and Fire Damage', *Fire Technology*, 49(3), pp. 709–739. doi: 10.1007/s10694-012-0289-2.

Mirza, O., Uy, B. and Krezo, S. (2011) 'Experimental Studies on the Behaviour of Headed Stud Shear Connectors for Composite Steel Concrete Beams under Elevated Temperatures', in. Research Publishing Services, pp. 467–473. doi: 10.3850/978-981-08-9247-0_rp066-icsas11.

NIST (2008) 'Structural Fire Response and Probable Collapse Sequence of the World Trade Centre Building 7', *Nist Ncstar 1-9*, 2. Available at: http://www.nist.gov/el/disasterstudies/wtc/wtc_finalreports.cfm.

Oehlers, D. J. *et al.* (1997) 'Partial Interaction in Composite Steel and Concrete Beams with Full Shear Connection', *Journal of Constructional Steel Research*, 41(2–3), pp. 235–248. doi: 10.1016/S0143-974X(97)80892-9.

Oehlers, D. J. and Bradford, M. A. (1995) *COMPOSITE STEEL AND CONCRETE STRUCTURAL MEMBERS*.

Qureshi, J. and Lam, D. (2012) 'Behaviour of headed shear stud in composite beams with profiled metal decking', *Advances in Structural Engineering*, 15(9), pp. 1547–1558. doi: 10.1260/1369-4332.15.9.1547.

Rackham, J. W. (2014) *Composite Slabs and Beams using Steel Decking: Best Practice for Design and Construction*.

Vasif Atilla Oven' (1996) "THE BEHAVIOUR OF COMPOSITE BEAMS WITH PARTIAL INTERACTION AT ELEVATED TEMPERATURES". School of Architectural Studies

Sengkwan Choi, Sanghoon Han, Sungbae Kim, Ali Nadjai, F. A. & J. C. (2009) *PERFORMANCE OF SHEAR STUDS IN FIRE*.

Shen, M. H. and Chung, K. F. (2017) 'Structural Behaviour of Stud Shear Connections with Solid and Composite Slabs Under Co-Existing Shear and Tension Forces', *Structures*, 9, pp. 79–90. doi: 10.1016/j.istruc.2016.09.011.

Wang, Y. C. (1998) 'Deflection of Steel-Concrete Composite Beams with Partial Shear Interaction', *Journal of Structural Engineering*, 124(10), pp. 1159–1165. doi: 10.1061/(asce)0733-9445(1998)124:10(1159).

Zaki, R., Butterworth, J. and Clifton, G. (2003) 'Shear Stud Capacity in Profiled Steel Decks', (January). Available at: http://e-book.lib.sjtu.edu.cn/nascc2004/data/contents/PSSC PDF Files/ShearStudCapinSteelDecks.pdf.

Zhao, B., Kruppa, J., "Experimental and numerical investigation of fire behaviour of steel and concrete composite beams," in ASCE-Composite Construction, Irsee, Germany, 1996.

Appendix

A- Capacity of the stud embedded in solid slab at normal temperature:

<u>A-1 19 mm × 100 mm studs in 30 MPa concrete (γ_v=1)</u>

Stud

$$R_{sc} = \frac{0.8\, f_u\, \pi\, d_{sc}^{\,2}}{4\gamma_v}$$

$$= \frac{0.8 \times 470.8 \times \pi \times 19^2}{4 \times 1} = 106.7 \text{ kN}$$

Concrete

$$f_{cm} = f_{ck} + 8$$

$$f_{cm} = 30 + 8 = 38 \text{ MPa}$$

$$E_{cm}(Gpa) = 22(\frac{f_{cm}}{10})^{0.3}$$

$$= 22(\frac{38}{10})^{0.3} = 32.836 \text{ GPa}$$

$$\alpha = 1 \ \text{ for } \frac{h_{sc}}{d_{sc}} > 4$$

$$R_{sc} = \frac{0.29\, \alpha\, d_{sc}^{\,2} \sqrt{f_{ck}\, E_{cm}}}{\gamma_v}$$

$$R_{sc} = \frac{0.29 \times 1 \times 19^2 \times \sqrt{38 \times 32.836 \times 10^3}}{1} = 104 \text{ kN}$$

A-2 22 mm × 100 mm studs in 30 MPa concrete (γ_v=1)

Stud

$$R_{sc} = \frac{0.8\, f_u\, \pi\, d_{sc}^2}{4\gamma_v}$$

$$= \frac{0.8 \times\, 470.8 \times\, \pi\, \times 22^2}{4 \times 1} = 143.17 \text{ kN}$$

Concrete

$$f_{cm} = f_{ck} + 8$$

$$f_{cm} = 30 + 8 = 38 \text{ MPa}$$

$$E_{cm}(\text{Gpa}) = 22(\frac{f_{cm}}{10})^{0.3}$$

$$= 22(\frac{38}{10})^{0.3} = 32.836 \text{ GPa}$$

$$\alpha = 1 \ \text{ for } \frac{h_{sc}}{d_{sc}} > 4$$

$$R_{sc} = \frac{0.29\, \alpha\, d_{sc}^2 \sqrt{f_{ck}\, E_{cm}}}{\gamma_v}$$

$$R_{sc} = \frac{0.29 \times\, 1 \times\,\, 22^2 \times \sqrt{38\, \times\, 32.836 \times 10^3}}{1} = 139.3 \text{ kN}$$

<u>A-3 16 mm × 75 mm studs in 30 MPa concrete (γ_v=1)</u>

Stud

$$R_{sc} = \frac{0.8\, f_u\, \pi\, d_{sc}^2}{4\gamma_v}$$

$$= \frac{0.8 \times 470.8 \times \pi \times 16^2}{4 \times 1} = 75.7 \text{ kN}$$

Concrete

$$f_{cm} = f_{ck} + 8$$

$$f_{cm} = 30 + 8 = 38 \text{ MPa}$$

$$E_{cm}(\text{Gpa}) = 22(\frac{f_{cm}}{10})^{0.3}$$

$$= 22 \times (\frac{38}{10})^{0.3} = 32.836 \text{ GPa}$$

$$\alpha = 1 \text{ for } \frac{h_{sc}}{d_{sc}} > 4$$

$$R_{sc} = \frac{0.29\, \alpha\, d_{sc}^2 \sqrt{f_{ck}\, E_{cm}}}{\gamma_v}$$

$$R_{sc} = \frac{0.29 \times 1 \times 16^2 \times \sqrt{38 \times 32.836 \times 10^3}}{1} = 73.68 \text{ kN}$$

B- Capacity of the stud embedded in composite slab at normal temperature:

B-1 19 mm × 100 mm studs in 30 MPa concrete with corrugated metal sheet oriented parallel to the steel beam

Reduction factor

$$\mathbf{k_t = 0.6 \frac{b_0}{h_p} \left(\frac{h_{sc}}{h_p} - 1 \right) \leq 1}$$

$$= 0.6 \times \frac{179}{76} \times \left(\frac{100}{76} - 1 \right) = 0.446$$

$$R_{sc} = 0.446 \times 104 \text{ kN} = 46.38 \text{ kN}$$

C- Capacity of the stud embedded in solid slab at elevated temperatures:

C-1 19 mm × 100 mm studs in 30 MPa concrete at 15 minutes

Stud

(Temperature of stud is taken as 80 % of flange temperature)

$$T°C \text{ stud} = 0.8 \times 484 \text{ °C} = 387°C$$

$$R_{sc,fi} = 0.8 \, k_{u,\theta} \, R_{sc}$$

$$= 0.8 \times 0.445 \times 106.7 = 38 \text{ kN}$$

concrete

(Temperature of concrete is taken as 40 % of flange temperature)

$$T°C \text{ concrete} = 0.4 \times 484 \text{ °C} = 193°C$$

$$R_{sc,fi} = k_{c,\theta} \, R_{sc}$$

$$= 0.9535 \times 104 = 99.16 \text{ kN}$$

<u>C-2 19 mm × 100 mm studs in 30 MPa concrete at 30 minutes</u>

Stud

(Temperature of stud is taken as 80 % of flange temperature)

$$\text{T°C stud} = 0.8 \times 700 \text{ °C} = 560\text{°C}$$

$$R_{sc,fi} = 0.8 \, k_{u,\theta} \, R_{sc}$$

$$= 0.8 \times 0.27 \times 106.7 = 23.04 \text{ kN}$$

concrete

(Temperature of concrete is taken as 40 % of flange temperature)

$$\text{T°C concrete} = 0.4 \times 700 \text{ °C} = 280\text{°C}$$

$$R_{sc,fi} = k_{c,\theta} \, R_{sc}$$

$$= 0.87 \times 104 = 90.48 \text{ kN}$$